Received: 22 February 2022 | Accepted: 9 July 2022

DOI: 10.1111/gcb.16345

Global Change Biology WILEY

RESEARCH ARTICLE

Mismatch of N release from the permafrost and vegetative uptake opens pathways of increasing nitrous oxide emissions in the high Arctic

Fabrice Lacroix[1,2,3] | Sönke Zaehle[1] | Silvia Caldararu[1] | Jörg Schaller[4] | Peter Stimmler[4] | David Holl[5] | Lars Kutzbach[5] | Mathias Göckede[1]

[1]Biogeochemical Signals (BSI), Max Planck Institute for Biogeochemistry, Jena, Germany

[2]Climate and Environmental Physics, University of Bern, Bern, Switzerland

[3]Oeschger Centre for Climate Change Research, University of Bern, Bern, Switzerland

[4]Leibniz Centre for Agricultural Landscape Research (ZALF), Müncheberg, Germany

[5]Institute of Soil Science, Center for Earth System Research and Sustainability (CEN), University Hamburg, Hamburg, Germany

Correspondence
Fabrice Lacroix, Biogeochemical Signals (BSI), Max Planck Institute for Biogeochemistry, Jena, Germany.
Email: flacro@bgc-jena.mpg.de

Funding information
Deutsche Forschungsgemeinschaft, Grant/Award Number: 390683824, GO1380/3-1 and SCHA1322/12-1; Horizon 2020 Framework Programme, Grant/Award Number: 101003536, 647204 and 951288; Max-Planck-Gesellschaft

Abstract

Biogeochemical cycling in permafrost-affected ecosystems remains associated with large uncertainties, which could impact the Earth's greenhouse gas budget and future climate policies. In particular, increased nutrient availability following permafrost thaw could perturb the greenhouse gas exchange in these systems, an effect largely unexplored until now. Here, we enhance the terrestrial ecosystem model QUINCY (QUantifying Interactions between terrestrial Nutrient CYcles and the climate system), which simulates fully coupled carbon (C), nitrogen (N) and phosphorus (P) cycles in vegetation and soil, with processes relevant in high latitudes (e.g., soil freezing and snow dynamics). In combination with site-level and satellite-based observations, we use the model to investigate impacts of increased nutrient availability from permafrost thawing in comparison to other climate-induced effects and CO_2 fertilization over 1960 to 2018 across the high Arctic. Our simulations show that enhanced availability of nutrients following permafrost thaw account for less than 15% of the total Gross primary productivity increase over the time period, despite simulated N limitation over the high Arctic scale. As an explanation for this weak fertilization effect, observational and model data indicate a mismatch between the timing of peak vegetative growth (week 26–27 of the year, corresponding to the beginning of July) and peak thaw depth (week 32–35, mid-to-late August), resulting in incomplete plant use of nutrients near the permafrost table. The resulting increasing N availability approaching the permafrost table enhances N loss pathways, which leads to rising nitrous oxide (N_2O) emissions in our model. Site-level emission trends of 2 mg N m^{-2} $year^{-1}$ on average over the historical time period could therefore predict an emerging increasing source of N_2O emissions following future permafrost thaw in the high Arctic.

KEYWORDS
carbon, climate, high Arctic, nitrogen, nitrous oxide, permafrost, vegetation

1 | INTRODUCTION

High-latitude permafrost-affected soils cover over one-sixth of the exposed northern hemisphere land surface and store vast amounts of carbon and nitrogen (Hugelius et al. 2013, 2020; Obu, 2021; Palmtag et al., in review). However, large uncertainties remain associated to the past and future perturbation of greenhouse gas fluxes in these regions, which could have an impact on achieving global climate targets (Biskaborn et al., 2019; Bruhwiler et al., 2021; Canadell et al., 2022; Natali et al., 2021; Schädel et al., 2018; Schuur et al., 2015). On the one hand, increased carbon fixation linked to enhanced vegetation growth in these regions has already been reported over the past few decades, with further drastic changes expected in the future (Canadell et al., 2022; Pearson et al., 2013; Winkler et al., 2019). On the other hand, the warming and thawing of frozen soils expose large organic carbon and nitrogen pools, which were conserved for thousands of years, to aerobic or anaerobic degradation, contributing to increased greenhouse gas emissions to the atmosphere (Burke et al., 2017; de Vrese & Brovkin, 2021; McGuire et al., 2018; Schädel et al., 2016; Schuur et al., 2015; Voigt et al., 2020). The feedback could be especially critical in the high Arctic, a region with disproportionate carbon and nitrogen stocks vulnerable to permafrost thaw (Hugelius et al., 2020; Palmtag et al., in review).

Since temperatures in Arctic regions have already increased substantially over the historical time period (Ballinger et al., 2020; Screen & Simmonds, 2010) and are projected to further increase in the future (Cai et al., 2021; Previdi et al., 2020), estimating the degree of permafrost thawing and its feedbacks on vegetation and soil carbon stocks is of high importance in the context of quantifying the greenhouse gas budget of high latitudes (Schuur et al., 2015). In addition to implications of climate warming for the exchange of greenhouse gases CO_2 and CH_4 in high latitudes, recent measurement campaigns have reported evident sources of nitrous oxide (N_2O) to the atmosphere from the high Arctic (Marushchak et al., 2021; Voigt et al., 2020; Wilkerson et al., 2019). Previously, N_2O emissions from the high latitudes were largely neglected in the global greenhouse gas budgets, owing to low nitrogen availability in the upper soil (Voigt et al., 2020). Strong uncertainty still exists with respect to the high-latitude N_2O flux for the present day (Marushchak et al., 2021; Voigt et al., 2020; Wilkerson et al., 2019), as well as in terms of its the future evolution of (Voigt et al., 2017).

The implications that changing climatic conditions and permafrost thaw have for vegetation and microbial dynamics in the high latitudes are still poorly constrained. In particular, the perturbations that the thaw of permafrost may impose on nutrient cycles in these regions are largely unexplored (Beermann et al., 2017; Chadburn et al., 2017). Since Arctic tundra ecosystems are usually strongly nutrient-limited (Finger et al., 2016; Haag, 1974; Natali et al., 2012; Pedersen et al., 2020; Street & Caldararu, 2022), increased nutrient mobilization from permafrost layers could potentially enhance vegetation growth through plant uptake and/or microbial activity. Such fertilization effects have been demonstrated in a variety of Arctic site-level investigations (Blume-Werry et al., 2019; Pedersen et al., 2020; Street et al., 2018; Yang et al., 2021). Large stocks of highly labile nitrogen are reported in the high-Arctic permafrost (Fouché et al., 2020; Hugelius et al., 2020; Salmon et al., 2016; Palmtag et al., in review), which would likely be rapidly degraded to biologically-available compounds upon soil thaw.

The fate of nitrogen (N) mobilized following permafrost thaw remains largely uncertain, despite being a strong limiting element for permafrost ecosystems (Haag, 1974; Natali et al., 2012; Pedersen et al., 2020). Both plants and microbes compete for the sparse N in the shallow active soil layer (Monteux et al., 2020). It is debated to which degree increased N release in the deeper soil, for instance owing to thaw of permafrost, would be taken up by the vegetations, thus retaining newly released N within the biosphere (Beermann et al., 2017; Blume-Werry et al., 2019; Finger et al., 2016; Keuper et al., 2017; Koven et al., 2015; Natali et al., 2012; Norby et al., 2019; Pedersen et al., 2020), used by microbes and potentially outgassed as N_2 and N_2O (Elberling et al., 2010; Voigt et al., 2017, 2020), or exported laterally (Rasmussen et al., 2022; Treat et al., 2016). Phosphorus (P) could also provide an important constraint for plants and microbial activity in high-latitude ecosystems (Salmon et al., 2018; Schaller et al., 2019; Street et al., 2018; Yang et al., 2021; Zhang et al., 2014), thus its increasing availability could impact the degradation of organic matter in the deep soil.

Impacts of climate change on high Arctic terrestrial systems have been assessed in the past using terrestrial land surface models (e.g., de Vrese & Brovkin, 2021; de Vrese et al., 2021; Koven et al., 2015). However, important uncertainties in representing biophysical processes in these regions certainly still exist (Chadburn et al., 2017; Schädel et al., 2018; Yokohata et al., 2020). These approaches have, for one, largely omitted nutrient dynamics in the high latitudes and their impacts on vegetation growth and microbial activity. They have also used either coarse vertical distributions, or even only two layers, to represent vertical soil profiles at the global scale (Chadburn et al., 2017). Both these factors strongly limit the assessment of effects caused by thawing of the permafrost on vegetative growth and microbial activity, and thus of greenhouse gas exchange.

To advance the understanding of the fate of nutrients originating from permafrost thaw in the high Arctic, we enhanced the terrestrial biosphere model QUINCY (QUantifying Interactions between terrestrial Nutrient CYcles and the climate system) with additional modules addressing specific bio-physical features important in the high Arctic. Using this enhanced model version, in addition to site-level observational data, we analysed transient simulations over 1960 to 2018 to quantify the impacts that deepening of the active layer and increased nutrient availability have on vegetation dynamics and greenhouse gas exchange, with a particular focus on the fate of N upon thaw of permafrost and pathways leading to N_2O emissions.

2 | METHODS

We used observational data collected at the site level and performed site-level simulations over the Arctic Tundra for 1901–2018 with the

global terrestrial model QUINCY. We thereby aimed to improve the understanding of impacts caused by nutrients (N and P) mobilized following the thaw of permafrost, both for vegetation growth and greenhouse gas emissions. We implemented additional features in both plant and soil modules of QUINCY to better represent physical soil processes taking place in this cold region (i.e., soil freezing, snow and inundation) but also including specific soil conditions for permafrost-affected soils, as well as alterations to vegetation dynamics as a response to changes in the soil state (i.e., dynamic root depths). Using this extended model version, we performed sets of simulations to isolate effects arising from increased nutrient availability following permafrost thaw, other changes in climate, as well as CO_2 fertilization, while also using site-level observational data to verify our analysis when possible.

2.1 | The QUINCY model

The QUINCY terrestrial biosphere model simulates water and energy exchanges, as well as coupled C, N and P cycles in soil and vegetation (Thum et al., 2019). The model has already been applied and validated within a number of studies investigating nutrient cycles in vegetation and soils (Caldararu et al., 2020, 2022; Yu et al., 2020). It provides improvements compared to other terrestrial biosphere models used in global assessments (e.g., Canadell et al., 2022) through its state-of-the-art representation of vegetation dynamics (Thum et al., 2019; Text S1) and vertically explicit representation of N and P cycling (Caldararu et al., 2020; Thum et al., 2019; Figure 1; Text S2). The model also includes the production of N-containing gases N_2O and N_2 through nitrification and denitrification (Figure 1; Text S2). QUINCY discretises both soil physical parameters and biogeochemical pools in the vertical plane, which is highly relevant for permafrost-affected soils. Omitting or poorly representing nutrient cycles and vertical gradients in permafrost-affected soils have been identified as important reasons for the poor performance of global terrestrial biosphere models in the high latitudes (Chadburn et al., 2017).

The model accounts for five pools of soil organic matter, that is, structural, polymeric, and woody litter, fast and slow degrading soil organic matter, which have dynamic C to N stoichiometries (Table S1; Thum et al., 2019). Organic N is mineralized to ammonium (NH_4), which in turn can be further oxidized to nitrate (NO_3) under aerobic conditions (nitrification), both of which are dependent on temperature and soil moisture conditions (Table S1). Mineralization is constrained to nil at temperatures below zero. During nitrification, N_2O is produced at a fixed ratio of N nitrified. QUINCY computes uptake of NH_4 and NO_3 within the root zone dependently on available C for growth and tissue stoichiometry, and proportional to the current soil N availability and fine root distribution in the model (Table S1). Stored reserve N and dynamic stoichiometry within plants further allow the plants to adapt to fluctuations and low nutrient levels (Caldararu et al., 2020). Under anaerobic soil conditions, NO_3 can undergo denitrification, producing N_2O and N_2 at a fixed ratio, dependently on temperature (Table S1). Aerobic and anaerobic volume fractions of the soil are calculated as in Zaehle et al. (2011).

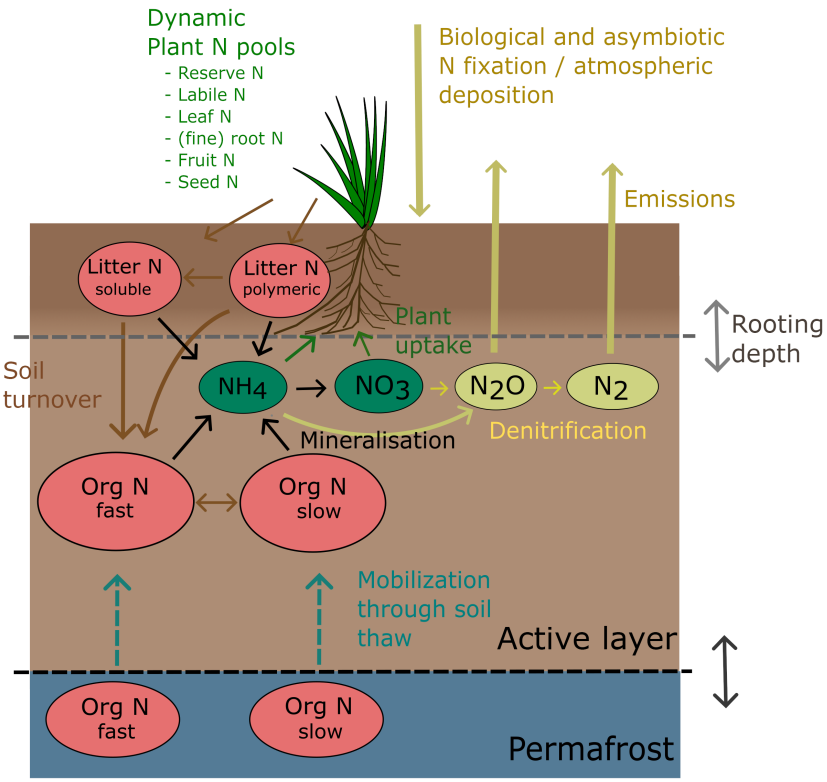

FIGURE 1 Conceptual scheme of N fluxes and pools in the QUINCY model extended for high-latitude processes. Note that our both active layer and the permanently frozen part of the soil comprise multiple model layers, and that the difference between rooting depth and permafrost table depth is exaggerated here. Atmospheric deposition inputs were also not considered in this study.

2.2 | Upgraded physical processes for high latitudes: Soil freezing, snow dynamics, organic matter effects, and inundation

To provide an improved representation of permafrost-affected ecosystems, we adapted the physical modules in QUINCY to account for effects of soil freezing and thawing, as well as of snow, on soil layer heat and water exchanges.

We extended the heat budget calculation with latent heat fluxes induced by soil freezing and thawing for every soil layer (Text S3). In similarity to other model implementations (Chadburn et al., 2015; Ekici et al., 2014), we assumed that a supercooled liquid water fraction remained present in the soil at freezing temperatures, which can also be observed in soil moisture measurements (Text S5). Additionally, water content is kept above the computed permanent wilting point in the surface soil layer for plant organs to survive the winter. The implementation of a multi-layer snow module (Text S4) served to represent the effects of snow coverage on the soil heat and water balance, preventing extreme cooling of the soil in the winter, while also delaying liquid water inputs to the soil until the melting season. Here, we used the same five-layer model structure as described in Ekici et al. (2014), with differences explained in Text S4.

We also accounted for the lower heat conductivity and higher specific heat capacity observed in soils with high organic contents, as often found in permafrost-affected soils. Similar to Burke et al. (2017), we used lower heat conductivity constants for the upper 30 cm of unfrozen soil, which is also where the highest soil organic carbon (SOC) contents are also simulated in the model and usually found in observations (Table S3).

We also implemented an inundation scheme to reproduce the retention of water over permanently frozen layers, which leads to saturated conditions in the spring/early summer as is the case in observations (Text S5; Göckede et al., 2019).

2.3 | Upgraded soil biogeochemistry for high latitudes: Initialisation and dynamics

Biogeochemical features in permafrost soils are unique in that organic material below the permafrost table is largely preserved, meaning that the permafrost stores stabile pools of carbon and nutrients. Achieving an initial vertical state of the soil adequate for the representation of permafrost gradients is challenging in terrestrial models (Chadburn et al., 2017), and many global terrestrial land surface models only resolve surface and subsurface soil as two layers. Here, we used 18 vertical layers up to a maximum depth of 9.5 meters, leading to layer thicknesses between 10 and 20 cm at the simulated permafrost table.

We initialised total SOC contents and organic soil C:N ratios at our two case study sites Cherskiy and Samoylov using measurements undertaken at these sites (Table S3, Zubrzycki et al., 2013). We used the land cover type estimations of Palmtag et al. (2022, in review) for the other high-Arctic sites. This approach quantifies specific Arctic land cover type carbon and N contents based on 651 soil pedons from 16 study areas. For all sites, we used the averaged C:N ratio over the entire vertical plane. We assumed 5% of soil organic matter to be fast degrading, a conservative estimate with respect to estimates of up to 10% (Hugelius et al., 2020; Strauss et al., 2015). To initialize organic P contents, we used the default organic N:P mole ratio of 55 used in Thum et al. (2019) for the global scale due to the lack of observational constraints.

The SOC contents were initialised to maintain a higher content and reactivity of organic carbon in deeper layers (Figure S1). This is not the case in the standard model, which prescribes exponentially decreasing SOC with depth, thus yielding close to zero contents at permafrost depths. The SOC was prescribed to follow fitted exponential distributions derived for Cherskiy ($k = -3.88\,cm^{-2}$) and Samoylov ($k = -0.009\,cm^{-2}$) in the first 50 cm, and constant past this depth as an approximated permafrost table. The SOC and organic N concentrations were then normalized using observations for the available estimates for 1–300 cm and 1–100 cm made for Cherskiy and Samoylov. Due to lacking data, we used an average of the two vertical distributions to determine the vertical distribution of the other sites, which was then normalized according to SOC contents taken from Palmtag et al. (in review). To preserve reactive SOC at permafrost depths, our simulations were initialized at negative temperatures to prevent its degradation during the model spin-up. We performed a spin-up simulation for the soil active layer to equilibrate to an approximately non-perturbed state with respect to human-caused warming (Figure S1). As a result, total SOC and N slightly deviate from observations that they were initialized for, especially in the top soil (Figure S1).

Due to the changes made to the soil hydrology as a result of soil freezing and inundation (Text S5), vertical leaching of biogeochemical compounds past the permafrost table is essentially inhibited in the model. Within the active layer, however, vertical transport of biogeochemical compounds can happen as a result of drainage, diffusion or due to bio-turbation.

2.4 | Upgraded vegetation dynamics for high latitudes: Timing of growth and frozen-soil-dependent root depth

In our model version, the start of the growing season was delayed by snow cover. The growing degree day count only began when snow coverage was less than the minimum coverage threshold, defined here as 2 cm snow thickness (Table S2).

Additionally, we developed a module that considers plant roots to be adaptive to the seasonal freezing and thawing of the soil. In this scheme, fine root growth is only possible in unfrozen soil layers at every model time step. Instead of using a fixed root distribution, we prescribed the root distribution used in the standard QUINCY model in the upper 30 cm of the soil, which dictates an exponential decrease of root mass with a decay constant of 5.5 m^{-1}, determined

for grasses by Jackson et al. (1996). This reflects that most roots in permafrost systems are found in shallow soil depths and do decrease with depth there (Blume-Werry et al., 2019; Finger et al., 2016; Iversen et al., 2015). Below 30 cm, we did not use a weighed profile, meaning that in these soil layers, root growth would happen at the same rate in all layers as long as they are not frozen. A major consequence of the dynamic root scheme is that nutrients stored within permanently frozen layers are unavailable for uptake by the plants. At the same time, nutrient pools at the bottom of the active layer only gradually become available for root uptake due to slowly increasing thaw depths during the summer.

2.5 | Simulation inputs, forcing, and strategy

We performed model simulations from 1901–2018 for 15 tundra sites of continuous permafrost over the high-Arctic region, represented by the C3 grass plant functional type in the model (Figure S2, soil parameters for every site are given in Supplement site_info_arctic_grasslands.csv). The model was driven with meteorological data from the University of East Anglia Climatic Research Unit Japanese Reanalysis (CRU-JRA; Harris, 2019), which is a reanalysis of incoming solar radiation, surface temperature, humidity, precipitation, surface pressure, and surface winds with the goal of providing atmospheric forcing for land surface models. The dataset is available at a spatial resolution of 0.5 × 0.5° and a 6-hourly temporal resolution. The atmospheric forcing data for our chosen sites were extracted from the CRU-JRA dataset according to their geographic coordinates, and the data were subsequently transformed to half-hourly timestep intervals using a weather generator (Zaehle & Friend, 2010). Furthermore, we used a vertical soil profile resolution of 18 layers, with increasing width down to a depth of 9.5 m. In our simulations, this set-up proved to be adequate for shallow permafrost table depths of 0.3–1.5 m that we simulated in the high Arctic.

We differentiated between effects of (i) atmospheric CO_2 fertilization, (ii) changes arising from perturbation of the climate, and (iii) increased availability of C, N and P from the permafrost on carbon cycle processes by conducting several sets of simulations for each high-Arctic site (Table 1). These simulations were performed after model spin-up periods of 300 years, which were driven with atmospheric conditions for 1901–1930, and were subsequently checked for important variable drifts. We conducted the first set of simulations (*climate + withoutpermafrostCNP*, Table 1), considering changes in climate, but initialising carbon and nutrients contents to exponentially decrease with depth, as in the standard model. By doing this, C, N and P contents at depth are close to zero, thus excluding any potential fertilization effect linked to a deepening active layer. The second set of simulations was again driven by changing climate (*climate*), but this time also considering the release of carbon and nutrient pools from previously permanently frozen layers, that is, release from the permafrost. The third set of simulations additionally considered the impact of increasing atmospheric CO_2 levels on vegetation dynamics and carbon cycle processes (*climate* + CO_2). To isolate the effects of increasing nutrients/carbon availability following permafrost thaw, other climate effects and CO_2 fertilization, differences between scenario simulation trends were computed.

Furthermore, we performed a simulation without the model implementations for high latitudes (*withoutHighLat*). To further elucidate effects caused by nutrient limitation, we conducted an additional simulation with the same atmospheric forcing conditions as *climate* + CO_2, but fixed soil N and P concentrations at fivefold their prescribed levels (*Nutrients5x*), values chosen during test simulations with the goal of largely alleviating nutrient-limiting conditions.

2.6 | Case study sites and observation datasets

We examined detailed results, including the evolution of biogeochemical fluxes, for two Siberian tundra sites with underlying continuous permafrost: Cherskiy (CHE) and Samoylov (SAM). The sites were chosen due to availability of datasets for soil conditions (soil temperature, snow depths, soil moisture, SOCC, and soil N), as well as eddy-covariance-based Gross primary productivity (GPP) estimates, to validate our results.

The Cherskiy site is located in Northeastern Siberia, in proximity to the Kolyma River. Mean annual temperature is around −11°C (Göckede et al., 2017). Underneath an organic peat layer of around 20 cm, silty loam can be found up to the permafrost table depth of

TABLE 1 Overview of simulations and their drivers

Simulation/driver	CO_2 fertilization	Climate	Permafrost carbon and nutrients	Further features
Main simulations				
climate + withoutpermafrostCNP		X		
climate		X	X	
climate + CO_2	X	X	X	
Comparison simulations				
withoutHighLat	X	X		Without soil freezing, snow dynamics and inundation model implementations
Nutrients5x	X	X		Soil N and P held constant at 5-fold prescribed values

around 60 cm. Vegetation near the site is dominated by tussock-forming species (Kittler et al., 2016). Soil temperature, snow depths, soil moisture and eddy-covariance fluxes for GPP were obtained as described in Kittler et al. (2016) and Göckede et al. (2017). Vertical profiles of SOC and total N were measured at the site and are provided in Table S3.

The Samoylov site is a river terrasse situated on an island of the Lena River delta. While the organic layer near the site can be up to 30 cm in thickness, it is typically less than 10 cm on the dry polygon rims due to differing hydrological conditions (Boike et al., 2018, 2019). The active layer is found at around 50 cm depth in mid-August, and the permafrost depth extends to over 400 m below the surface. Vegetation coverage is dominated by sedges and mosses, dwarf shrubs and forbs (Kutzbach et al., 2004, 2007). We used soil temperature and snow depth measurements at the site reported in Boike et al. (2019) for the validation of our model and estimations of thaw depths. We constructed eddy-covariance GPP estimates for 2014–2017 based on CO_2 exchange product of Holl et al. (2019), applying a refined version of the bulk model approach of Runkle et al. (2013; Text S6). SOC and total soil N content measurements were taken from Zubrzycki et al. (2013).

In addition to the site-level data, we also compared modelled GPP to the MOD17A2H MODIS/Terra Gross Primary Productivity product (Running et al., 2015), which was extracted for the geographic coordinates of the individual sites at the original 500 m resolution.

2.7 | Analysis strategy

We analysed trends in fluxes and temperatures for the time frame 1960–2018 via linear regression, computing statistical significance through Student's *t*-tests, and multiplying the yearly trend with the entire analysis timespan. This timeframe was chosen due to the substantial increase in observed temperature past the 1960s. We also calculated weekly averages for the time period 1950–1970, which we assumed to be largely unperturbed, and the perturbed present-day timeframe 1998–2018, to compare the seasonal dynamics of the two time slices.

3 | RESULTS

3.1 | Soil temperature and active layer depths

Simulated seasonal soil temperatures in the model are in good agreement with observed temperatures over a multi-year average when including the model extensions for high-latitude processes (Figure 2). The model reproduces seasonal temperature fluctuations in the top soil (6–8 cm, Figure 2a,b) and in the deeper soil (60–64 cm, Figure 2e,f), where soil temperature remains near the freezing point for an extended time period in the summer. Our simulations still yield positive summertime biases of 3–6°C for 6–8 cm and 28–32 cm at both Cherskiy and Samoylov sites, while simulated winter soil temperatures are too high at the Samoylov site.

Simulated mean maximum thaw depths of 0.7 and 0.6 m adequately reproduce averaged observed maximum thaw depths of 0.5–0.7 m and 0.4–0.6 m at Cherskiy and Samoylov, respectively (Boike et al., 2019; Göckede et al., 2017). Snow seasonality is reasonably represented over the year, although snow depth is overestimated at Samoylov and underestimated at Cherskiy with respect to observational data (Figure S4). The model struggles at estimating magnitudes of water content fluctuations and field saturation capacity; however, it reproduces low soil moisture in the winter period and majorly saturated conditions in the deeper soil over the entire summer (Figure S3).

3.2 | Mismatch of GPP and soil thaw peaks

Simulated annual GPP at Cherskiy and Samoylov amount to 353 and 107 g C m^{-2} $year^{-1}$ in the *climate* + CO_2 simulation over a multiple year mean (Figure 3a,b), respectively. For the same sites, our eddy-covariance derived products provide annual mean GPP estimates of 321 and 134 g C m^{-2} $year^{-1}$, and the MODIS-based product quantifies annual mean GPP of 266 and 125 g C m^{-2} $year^{-1}$ (Figure 3a,b; Figure S5). Over the pan-Arctic scale, we compute an average GPP of 307 g C m^{-2} $year^{-1}$ and find good agreement of modelled GPP with the MODIS dataset on the individual site level (r^2 = .72, Figure S6), although it should be noted that our model performs better than the MODIS product when comparing to eddy-covariance based magnitude and seasonal variations of GPP for the two sites we analysed (Figure S5). Modelled annual GPP in *climate* + CO_2 is 3-fold lower on average than in the simulations *Nutrients5x* (Figure S7), emphasizing that soil nutrient levels are limiting GPP in *climate* + CO_2 and provide a strong constraint for reproducing observed GPP at the site level.

Our model performs well overall in terms of reproducing peak and seasonal variation of site-level GPP over multi-year means for both case-study sites with respect to the eddy-covariance estimates (Figure 3a,b). The weekly averaged simulated GPP peak is reached during week 27 on average at both case study sites (end of June), at magnitudes of 4.9 µmol m^{-2} s^{-1} (Cherskiy) and 1.6 µmol m^{-2} s^{-1} (Samoylov). Over all Arctic sites, the GPP peak is also reached at week 27 on average, at an Arctic-average GPP level peak of 3.7 µmol m^{-2} s^{-1}. After reaching this peak, GPP at both case study sites sharply declines in both the eddy-covariance products observations and in the model (Figure 3a,b). The seasonality found in the monthly averaged MODIS dataset also suggests a GPP peak early in the summer (Figure S5). Our model also indicates that GPP decreases past the peak owe to depletion of soil N, since modelled soil N availability cannot meet plant N demand at week 26 at Cherskiy and at week 27 at Samoylov over the multi-year year average (Figure S7). Averaged over all high-Arctic sites, plant N demand exceeds N soil availability at week 26 (Figure S8). This is in concurrence with declines of both simulated and observed GPP.

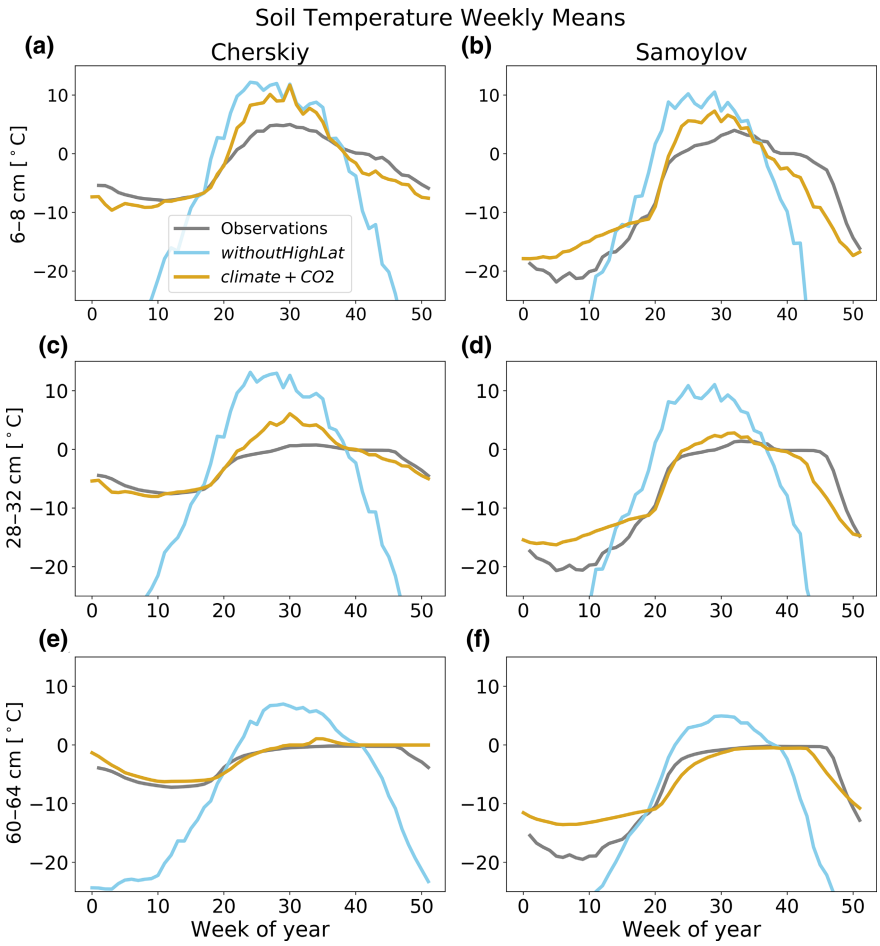

FIGURE 2 Weekly mean observed and modelled soil temperature, without high-latitude processes (*withoutHighLat*) and with (*climate* + CO_2) permafrost-specific implementations. Panels a,b show soil temperature at 6–8 cm, panels c,d 28–32 cm and panels e,f 60–64 cm depths at Cherskiy (left panels) and Samoylov (right panels), averaged over 2015–2018 and 2009–2014 for Cherskiy and Samoylov, respectively.

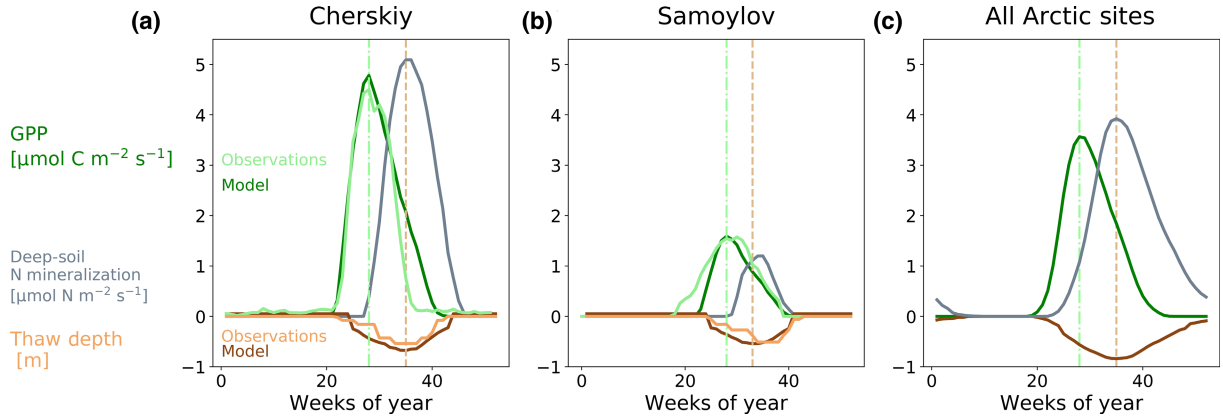

FIGURE 3 Weekly mean Gross primary productivity (GPP) and thaw depth climatology averaged over 1998–2018 in the *climate* + CO_2 simulation (model) and in observations at (a) Cherskiy (2015–2018), (b) Samoylov (2014–2018) and (c) averaged over all Arctic sites (no observation values given). Additionally, the simulated weekly deep-soil (50–100 cm) N mineralization climatology is shown in gray. Observed thaw depths were computed by finding the depth of the freezing point from the observed soil temperature profile. This was computed by linearly interpolating between measurements at different depths at the sites. Point-dotted green and pointed light brown lines indicate the timing of the GPP peak and of maximum soil thaw, respectively.

Both observational data and model simulations show seasonal thawing maxima succeeds the GPP maxima by several weeks at both case study sites, as well as for the Arctic average (Figure 3a,c). In our multi-year averaged observational data, where we derived the soil thaw depth through interpolation of the temperature between the coarsely measured layers, we find maximum thaw depths of 0.7 and 0.6 m at weeks 34 and 33 and at Cherskiy and Samoylov on average, respectively. The model reflects this pattern, simulating the same maximum thaw depth at weeks 35 and 34, respectively. The timing of maxima N mineralization, or N release, in the deep soil (50–100 cm), occurs in concurrence with or closely following the thaw depth maxima in the model (Figure 3a,c).

3.3 | Perturbation of active layer depth and increased deep-soil nutrient availability

Our observation-based forcing dataset prescribes rising atmospheric CO_2 levels, from 312 ppm in 1960 to 409 ppm in 2018, as well as annual mean surface temperatures, rising by 2.3 and 2.5°C over 1960–2018 for the Cherskiy and Samoylov sites, respectively (Figure 4a,d,h). The perturbation of heat exchange between atmosphere and soil surface is also reflected through warming rates in simulated annual mean upper-soil temperatures (30 cm), which show increases of 1.6 and 2.0°C at the both sites. Over the same time period and all Arctic sites, atmospheric temperatures rise by 2.4°C, leading to a soil temperature increase of 2.1°C at 30 cm depth. The warming impacts the depth of the permanently frozen layer in our simulations, with the active layer depth increasing by 0.19 and 0.15 m over 1960–2018 due to increased thaw at Cherskiy and Samoylov, respectively, and by 0.20 m at the high Arctic average (Figure 4b,f,j). Based on SOC contents averaged for the period 1950–1970 in *climate* + CO_2, these increases in active layer depth would expose 1.4–6.9 kg C m^{-2} $year^{-1}$ to potential degradation over 1960–2018 (low value for Samoylov, high value for Cherskiy), of which 71–338 g C m^{-2} $year^{-1}$ is fast-degrading. Following exposure of permafrost carbon to non-freezing temperatures, soil respiration increases by 105 and 26 g C m^{-2} $year^{-1}$ at Cherskiy and Samoylov, with the deep soil (50–100 cm) responsible for 21 and 5 g C m^{-2} $year^{-1}$ of the increase. Over all Arctic sites, the soil respiration increase is of 66 g C m^{-2} $year^{-1}$, with deep-soil respiration increasing by 13 g C m^{-2} $year^{-1}$. The shallowest layer of the deep-soil vertical range (~50 cm) is only exposed to above-zero temperatures for 2–6 weeks of the year (low value for Samoylov, high value for Cherskiy) over 1998–2018 on average.

Soil thaw simulated by the model also exposes 5.9 and 21 g N m^{-2} $year^{-1}$ and 2.0 and 9.4 g P m^{-2} $year^{-1}$ of fast-degrading organic N and P at Cherskiy and Samoylov, respectively, to temperatures above zero, and thus mineralisation. Over the Arctic mean, the increases in active layer depth over the 1960–2018 time period increase organic N and P mineralization by 0.6 and 0.2 g N m^{-2} $year^{-1}$ and 0.01–0.03 g P m^{-2} $year^{-1}$ in the deep soil aggregated over the time span at Cherskiy and Samoylov, respectively. Averaged over

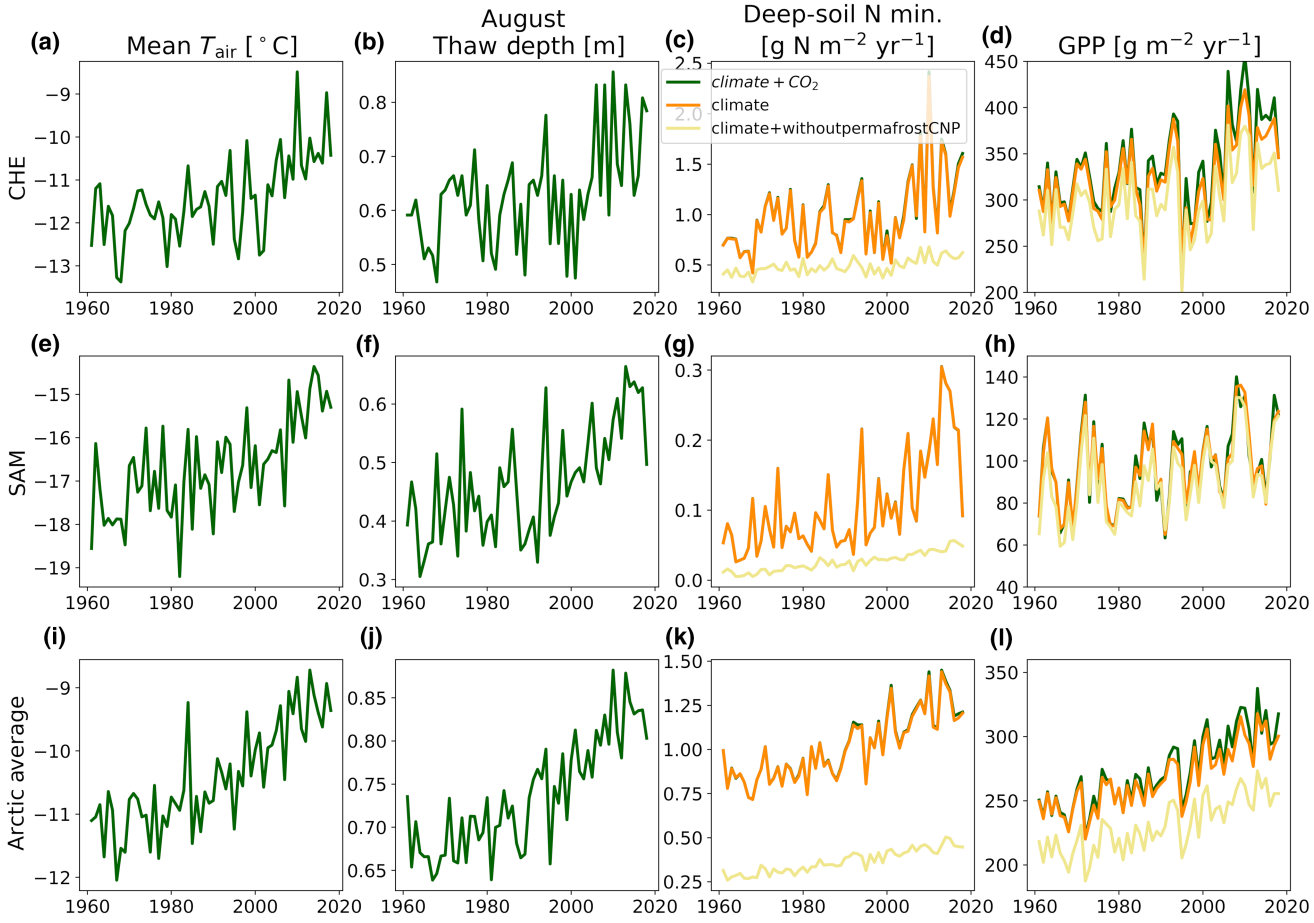

FIGURE 4 Temporal evolution of annual mean air surface temperature (left column, panels a,e,i), simulated average August thaw depth (middle left, panels b,f,j), simulated annual N mineralization from 50 to 100 cm (deep-soil N min., middle right, panels c,g,k) and simulated annual Gross primary productivity (GPP) (right column, panels d,h,l) over 1960 to 2018. Deep-soil min. and GPP are shown for simulations considering CO_2 fertilization and climate perturbations (*climate* + CO_2), as climate perturbations alone (*climate*) and climate perturbations without permafrost carbon and nutrient initialisations (*climate* + *withoutpermafrostCNP*) at Cherskiy (CHE), Samoylov (SAM) and averaged over all high Arctic sites.

all sites, we compute an increase of 0.6 g N m^{-2} $year^{-1}$ and 0.04 g P m^{-2} $year^{-1}$ of organic N and P mineralization for the same time period. In the case of N, this means a steep 2-to-3-fold increase with respect to 1950–1970 organic N mineralization levels, which were close to zero (Figure 4c,g,k). In the case of P, the net transformation of mineral-bound P to biologically available P increases by 0.06–0.19 g P m^{-2} $year^{-1}$ in the deep soil at the Arctic average.

As a result of the deepening of the active layer, annual mean root carbon content undergoes a strong relative increase at depths of 50–100 cm (+0.3 g C m^{-2}, or +156% in relative terms). Overall, however, the root carbon distribution only experiences minor changes in our simulations when comparing the beginning of the 1960s with present-day conditions, with around 85% of roots still simulated in the upper 20 cm of the soil (Figure 5a–c) for 1998–2018. Root growth past 50 cm is inhibited to 2–6 weeks during the year due to freezing temperatures in the deep soil.

Plant nutrient uptake in the deep soil is enhanced by 0.6 and 0.1 g N m^{-2} $year^{-1}$, and 0.06 and 0.09 g P m^{-2} $year^{-1}$ at Cherskiy and Samoylov, respectively, over the simulation time period (Figure 5d–f). Averaged over all sites, deep-soil plant nutrient uptake increases by 0.3 g N m^{-2} $year^{-1}$. This leads to a total mismatch in 1998–2018 deep-soil N mineralization of 1.2 and 0.2 g N m^{-2} $year^{-1}$ and 1998–2018 plant N uptake of 0.3 and 0.1 g N m^{-2} $year^{-1}$ at Cherskiy and Samoylov, respectively (Figure 5d–f). Averaged over the high-Arctic scale, mean 1998–2018 deep-soil N mineralisation is 1.1 g N m^{-2} $year^{-1}$ and plant N uptake is 0.6 g N m^{-2} $year^{-1}$. Our results suggest that, averaged over all Arctic sites, around 40%–60% of N mineralised in the deep soil is taken up through plant uptake over the course of a year for the 1998–2018 time slice. Due to the mismatch of N and P release and plant uptake in the deep soil, our model also simulates a vertical gradient in nutrient availability increasing towards the permafrost front for 1998–2018 (Figure S9).

3.4 | Implications for GPP compared with other perturbations

Our simulations indicate an increase in GPP for all case-study sites over 1960–2018 in the *climate* + CO_2 simulation, as result of all perturbations (Figure 4d,h,l). Increased nutrient availability from the thawing of permafrost thereby contributes to GPP increases of 9 and 5 g C m^{-2} $year^{-1}$ aggregated over the entire 1960–2018 timespan at the Cherskiy and Samoylov sites, and 10 g C m^{-2} $year^{-1}$ on average over all Arctic sites (Figures 6 and 9). Other climate-induced changes account for increases in the GPP of 58 and 32 g C m^{-2} $year^{-1}$ at both sites, and 57 g C m^{-2} $year^{-1}$ at the Arctic scale. Alone, CO_2 fertilization accounts for rising the GPP by only 18 g C m^{-2} $year^{-1}$ at Cherskiy, and a non-significant effect at Samoylov. Over the high-Arctic average, GPP increases by 11 g C m^{-2} $year^{-1}$. At the Cherskiy and Samoylov sites, GPP trends arising from all perturbations account for a total increase in GPP of 84 and 37 g C m^{-2} $year^{-1}$ aggregated, respectively. Averaged over all Arctic sites, the GPP increase resulting from all perturbations is of 79 g C m^{-2} $year^{-1}$. These changes represent increases of 30% and 27% with respect to 1950–1970 mean levels at our case study sites, and a 36% increase at the high Arctic scale. Climate-induced effects (including increased nutrient availability due to permafrost thaw) overall account for over 70% of the total GPP change in all cases at the high Arctic scale, while increased nutrient availability following permafrost thaw, and CO_2 fertilization, account for around 15% of the GPP increase each.

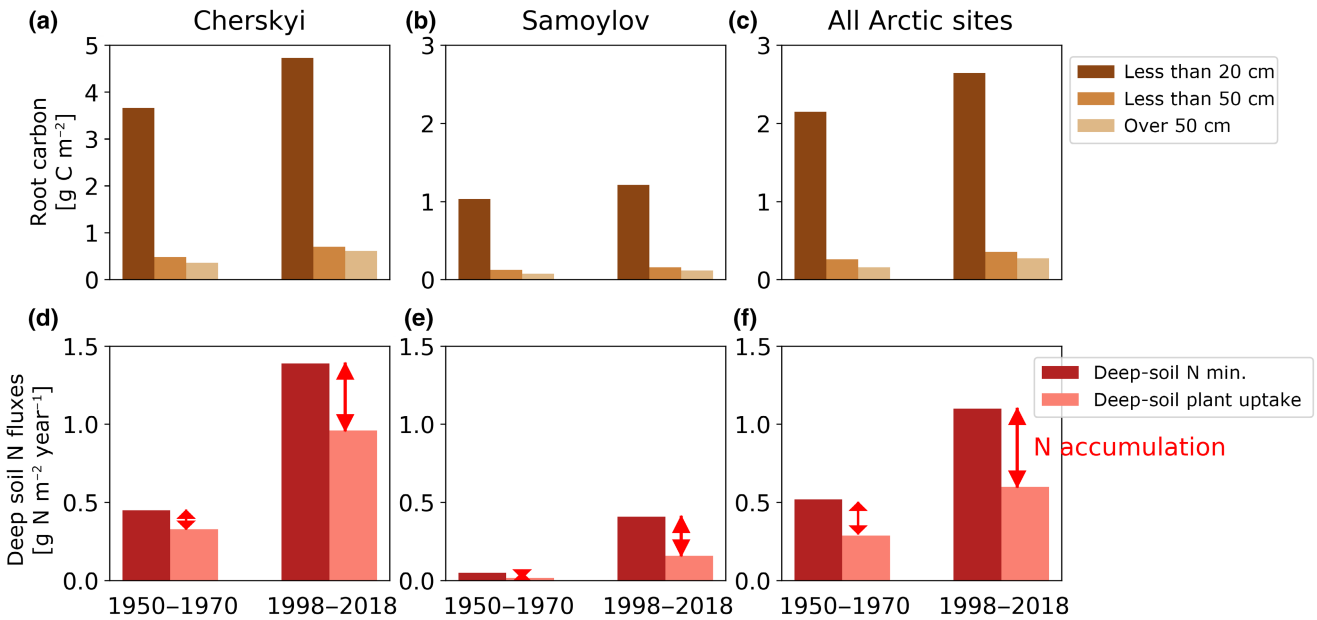

FIGURE 5 Panels a–c show mean root carbon and panels d–f show annual mean deep-soil (50–100 cm) N mineralization (deep-soil N min) and plant N uptake (plant N uptake) at Cherskiy, Samoylov and averaged over all Arctic sites, over 1950–1970 and 1998–2018.

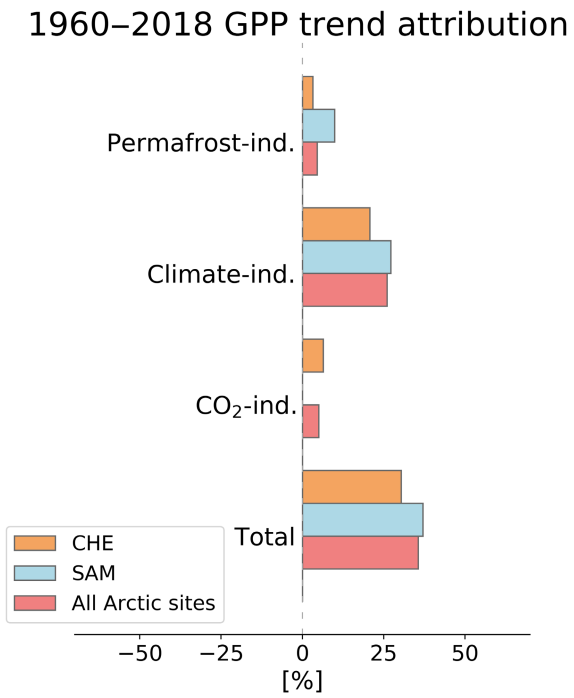

FIGURE 6 Statistically significant relative trends in site Gross primary productivity (GPP) induced by increased permafrost C, N and P availability (permafrost-ind.), other climate-induced perturbations (climate-ind.), CO_2-fertilization (CO_2-ind.) and total changes (Total), relative to 1950–1970 GPP averages.

3.5 | Implications for N loss pathways and N_2O emissions

Since newly mineralized N from previously frozen organic soil layers is not completely removed from the deep soil through plant uptake (Figure 5), solute N concentrations increase at the permafrost front (Figure S9). This leads to increasing deep-soil loss pathways of N (i.e., nitrification, denitrification, and transport) in the *CO_2 + climate* simulation. At Cherskiy and Samoylov, we compute increases in nitrification of 166 (+10%) and 95 (+25%) mg N m^{-2} $year^{-1}$, and of 77 (+44%) and 14 (+40%) mg N m^{-2} $year^{-1}$ in denitrification over the simulation time period, respectively. At the high Arctic average, we compute an increase in nitrification of 138 mg N m^{-2} $year^{-1}$ (+12%) and an increase in denitrification of 43 mg N m^{-2} $year^{-1}$ (+25%). Both increases in nitrification and denitrification occur in concurrence to the period of deepest thaw depths in the model (Figure 7a–c). The increases in nitrification and denitrification cause a simulated rise in N_2O fluxes of 1.6 and 0.4 mg N m^{-2} $year^{-1}$ to the atmosphere at Cherskiy and Samoylov, respectively, leading to present-day fluxes of 5.2 and 1.1 mg N m^{-2} $year^{-1}$ for 1998–2018 (Figure 8b–d). Over all high-Arctic sites the 2.2 mg N m^{-2} $year^{-1}$ mean increase in N_2O emissions lead to contemporary emissions of 3.5 mg N m^{-2} $year^{-1}$. This suggests an increase of more than 50% over all sites over 1960–2018 at the Arctic average. The growing season emissions computed by our model compare well to median emissions observed by Marushchak et al. (2021) for the Yedoma domain in Eastern Siberia, and is situated within the wide range of estimates made until now for the Arctic (Figure 8e).

N_2O emissions and their trends over 1960–2018 are higher in *climate + CO_2* than in *climate + withoutpermafrostCNP*, which does not consider increased N availability via the mobilization of permafrost pools, at both case study sites and at the high Arctic average (Figures 8b–d and 9c). While denitrification and nitrification are enhanced shortly before or following soil thawing peaks, increased N_2O emissions occur later when the deep-soil re-freezes during weeks 40 to 42. This is also the timeframe when the deep soil is aerated again in the model during freezing (Figure S2). Overall, the months of September and October account for over half of total yearly N_2O emissions averaged over all sites for 1998–2018.

The magnitude of N_2O emission rise shows an increasing relation with prescribed total soil N (Figure 10a). The magnitude in the site-level N_2O emissions trend is also dependent on degree of soil thaw, with increasing soil thaw seemingly leading to increasing N_2O emissions (Figure 10b). Indeed, our model shows a stronger response of N_2O emissions to increasing thaw depths than for GPP (Figure 10b). We also show significant correlation in the simulated year-to-year magnitude of the N_2O fluxes shows with surface air temperature (2 m) at Cherskiy (0.39) and Samoylov (0.5).

4 | DISCUSSION

4.1 | Modelling the terrestrial biosphere of high latitudes in QUINCY

Estimating human-caused changes in greenhouse gas exchanges over time is presently strongly dependent on global land surface models (Canadell et al., 2022; Friedlingstein et al., 2020). The representation of high-latitude biophysical processes in these models is, however, still associated with strong limitations. Models have, for one, been lacking in terms of their vertical representation of physical and biogeochemical features in permafrost-affected soils (Schädel et al., 2016). Second, nutrient cycles in high latitudes are either omitted or strongly simplified in these models (Chadburn et al., 2017), even though both N and P impose important constrains for microbial and vegetation dynamics in the high latitudes (Finger et al., 2016; Haag, 1974; Natali et al., 2012; Pedersen et al., 2020; Schaller et al., 2019; Yang et al., 2021). Through the full vertical discretization of both physical and biogeochemical variables, our extended QUINCY model version permits the analysis of changes associated with vertical permafrost thaw and their impact on vegetation and soil dynamics, while also taking into account a full representation of C, N and P cycles. Our model representation of dynamic changes in root distributions following soil thaw offers a simple, yet improved formulation to assess impacts of changing long-term and seasonal soil conditions on vegetation growth and increased nutrient availability in the deep soil. Until now, only strongly simplified impacts of N release from the permafrost have been assessed using bucket-type approaches (Beermann et al., 2017), whereas we offer an improved dynamic representation of the interaction of permafrost

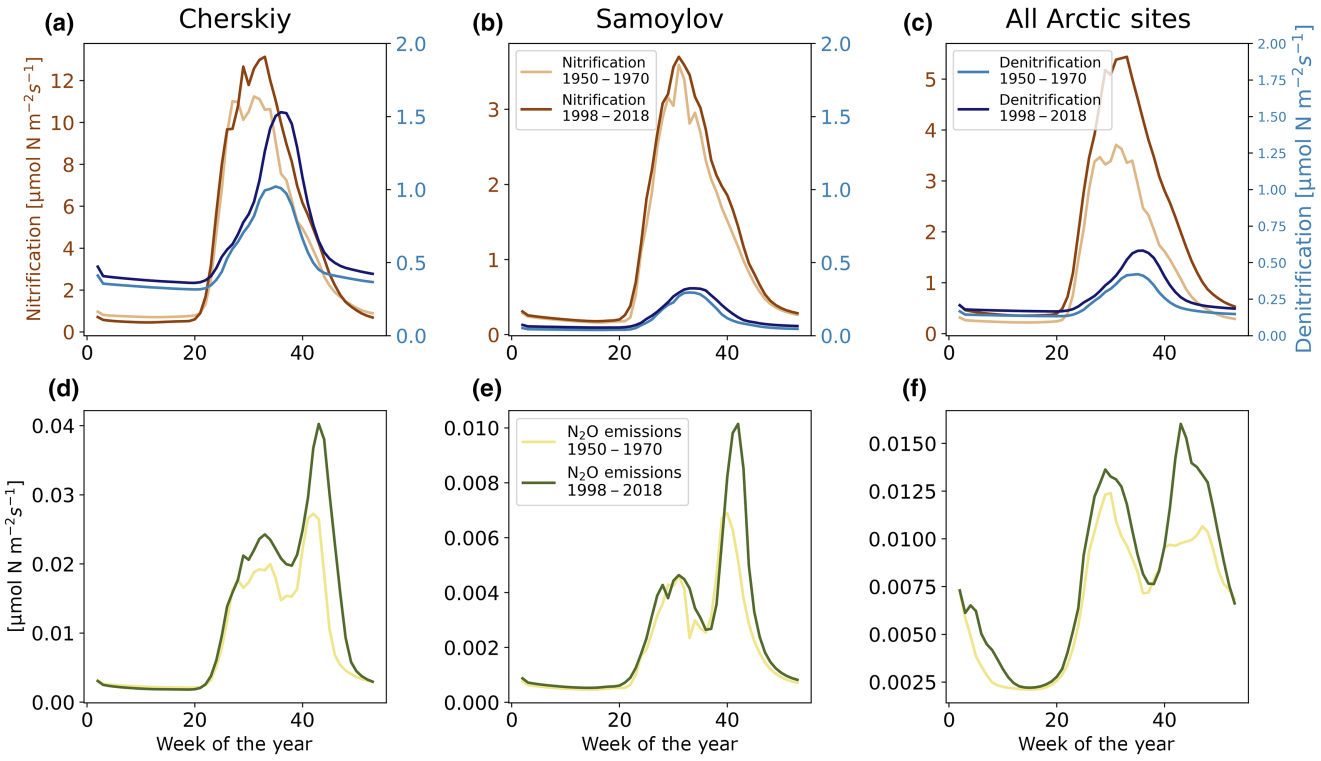

FIGURE 7 Weekly mean nitrification and denitrification rates (a–c), as well as weekly mean N_2O emission rates (d–f) averaged for 1950–1970 and 1998–2018 at Cherskiy, Samoylov and averaged over all Arctic sites.

thaw, increased C-N-P mobilization following the thaw, and vegetative uptake and microbial dynamics.

The model presented here still has clear limitations in its biophysical representation of high-latitude permafrost ecosystems. Strong simplifications are made in both physical soil processes, as well as vegetation dynamics. The parametrizations implemented here are often of first order, with organic matter mineralization for instance being constrained by a singular rate constant in combination with a temperature and soil moisture scaling factor. While parameters in our model have been assessed in terms of representing important land surface variables at the global scale (e.g., Thum et al., 2019), as well as the assessments for permafrost-affected soils we provide in this study, improvements in quantifying both vegetative and soil processes both from observational and modelling perspectives are still needed in the high Arctic.

Important challenges remain in terms of representing soil moisture and energy fluxes associated with snow cover. These are largely community-scale problems, since land surface models struggle to represent the observed local conditions of these variables. In our study, we assume fixed constants for snow density, specific heat conductivity, and heat capacity, which are partly computed dynamically in other models (Chadburn et al., 2015; Guimberteau et al., 2018). We also assume soil heat conductivity and specific heat capacity also do not change dynamically as a response to soil water content and soil organic matter, which could lead to certain bias in soil temperatures. A further source of uncertainty arises from the handling of species composition in the model. Assuming homogenous grassland coverage could cause biases in GPP as shown for instance at the Samoylov site, where GPP is reported to be majorly affected by mosses (Holl et al., 2019). Such biases could potentially be reduced by improving the representation of Arctic plant functional types in global vegetation models (Sulman et al., 2021).

Our model only represents limited spatial heterogeneity, both in the vertical and horizontal plane, which is partly linked with the polygonal tundra landscape found at many sites. The heterogeneity in soil variables such as heat conductivity, even at the local scale (Boike et al., 2019; Göckede et al., 2019), could strongly impact the degree of thaw at these scales. Our results should thus be interpreted as the bulk mean of the spatial fluxes with a strong degree of local uncertainty, and also omitting non-linear effects such as landscape collapse following deep-soil thaw (e.g., Yang et al., 2021).

4.2 | Changes in vegetation growth due to increased nutrient availability from the permafrost compared with increases caused by other drivers

Over the past century, Arctic regions have been subject to disproportionate warming due to climate change (e.g., Serreze & Barry, 2011), which has been reported to already affect dynamics of vegetation in the high latitudes. Through our set of simulations, we can decompose total perturbations caused by increased nutrient and carbon availability through permafrost thaw, other climate effects (e.g., earlier growth season, higher atmospheric and soil temperatures) and CO_2 fertilization alone. Our computed GPP increase of around 40% for the 1960–2018 period is

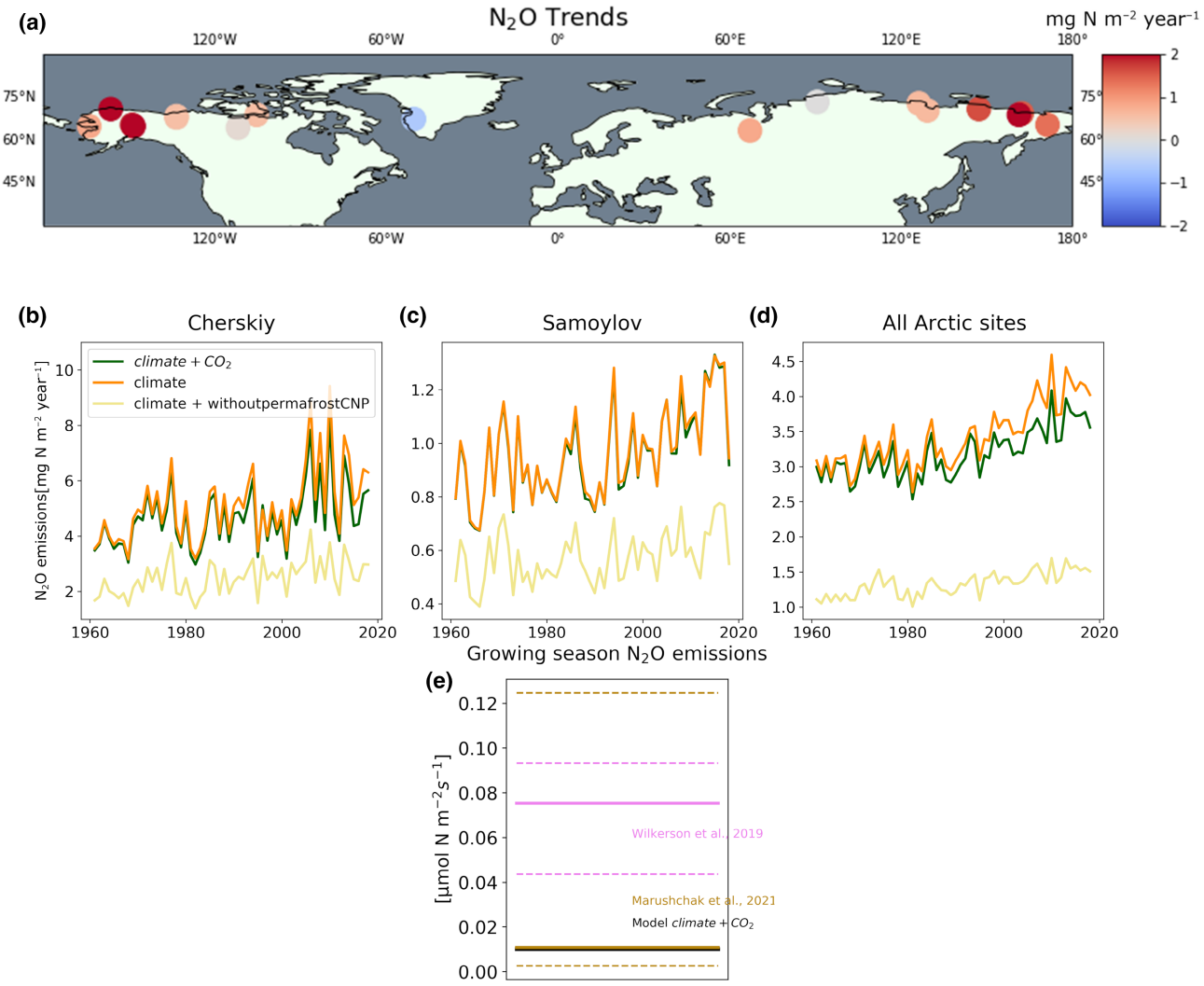

FIGURE 8 Panel (a) shows trends in N_2O emissions over all Arctic sites individually, aggregated over the 1960–2018 time span. Panel (b) shows the evolution of annual mean N_2O emissions over 1960–2018 at Cherskiy (b), Samoylov (c) and all high Arctic sites (d). Panel (e) shows averaged growing season (June–August) emission rates averaged over all Arctic sites in CO_2 + climate versus observed estimate means (solid lines) and upper and lower ranges (dashed lines) reported by Wilkerson et al. (2019) and Marushchak et al. (2021).

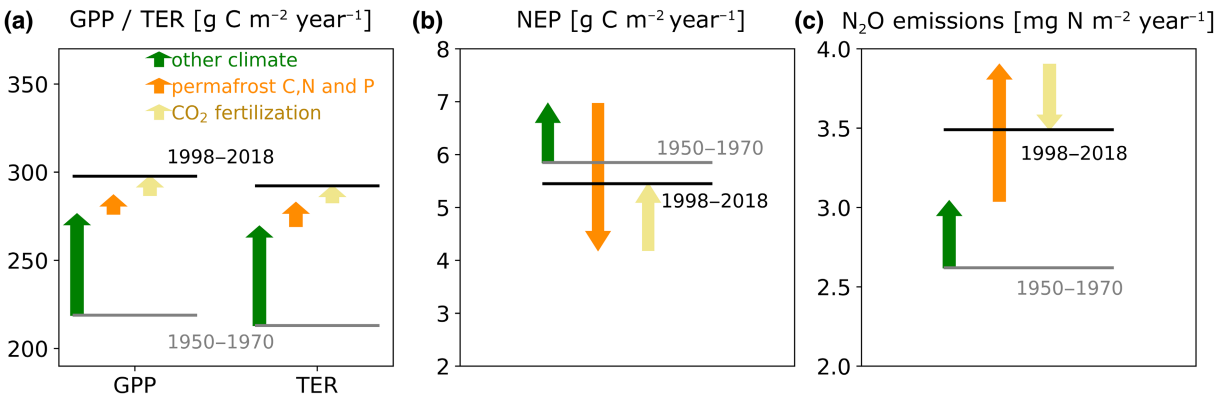

FIGURE 9 Simulated response of Gross primary productivity (GPP) and total ecosystem respiration (TER, panel a), net ecosystem production (NEP, panel b) and N_2O emissions (panel c) to climate effects other than increased permafrost nutrients and carbon (other climate, green), permafrost C, N, and P (orange) and CO_2 fertilization (khaki), all averaged over all sites.

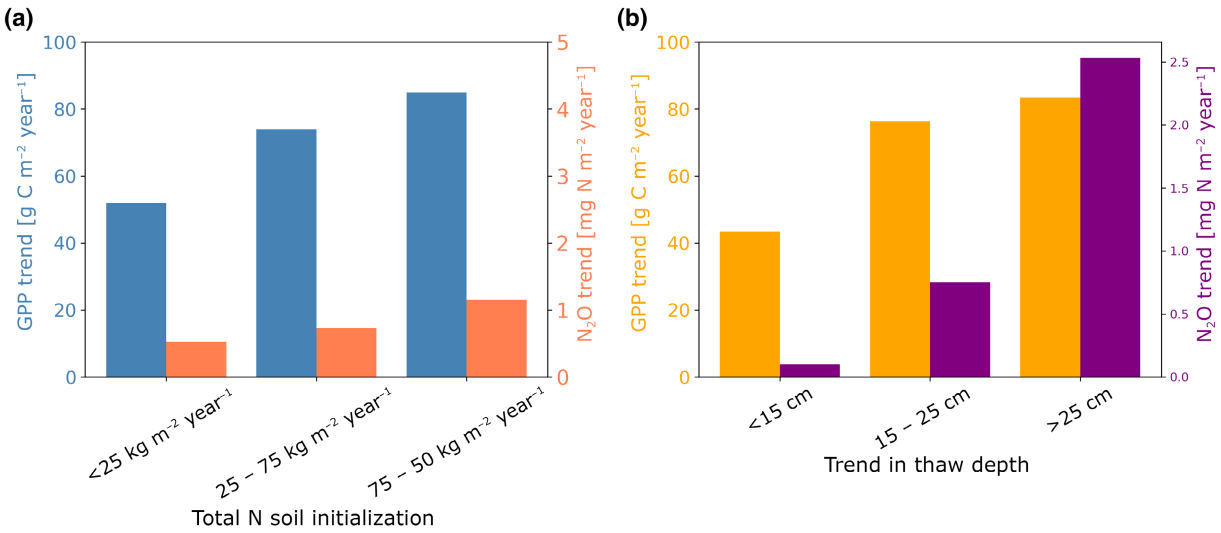

FIGURE 10 Averaged Gross primary productivity (GPP) and N_2O emission trends for sites with low (<25 kg N m^{-2} $year^{-1}$), mid (25–75 kg N m^{-2} $year^{-1}$), and high (>75 kg N m^{-2} $year^{-1}$) prescribed soil N initialisations (a), and less than 15 cm, 15–25 cm and over 25 cm trends in thaw depths over 1960–2018.

consistent with increases in greenness of around 10% per decade since the 1980s derived from satellite estimates (Winkler et al., 2019).

Our model suggests that increased nutrient input from permafrost thaw is responsible for less than 15% of the total GPP change over 1960–2018 at the high-Arctic scale. This effect could be increased the future, with increased thaw meaning further increases in nutrient supply, as well as longer growing season periods of potential vegetation uptake (Pedersen et al., 2020). Other climate effects have the largest effect on the simulated GPP trend over our investigated time period. Our results also suggest a trend towards a slightly earlier start and peak of the growing season with our simulations showing a 2 weeks earlier growing season peak of GPP at Cherskiy, and 1-week earlier peak at Samoylov and at the Arctic scale over the 1960 to 2018 period (Figure S10). This feature is in agreement with the study of Park et al. (2019), who report a historical trend in start and peak of vegetation growth of 1 day per decade derived from a satellite-based approach. CO_2 fertilization plays only a small role in explaining the GPP increase at the Arctic scale in our model, which likely owes to vegetation growth being strongly N limited at our case-study sites, which is also confirmed by the simulated GPP trend being dependent on total soil N.

4.3 | Root dynamics as response to deep-soil thaw and incomplete use of deep-soil N

Ecosystems in the Arctic tundra are reported to be strongly nutrient-limited during the growing season (Martin et al., 2022; Schuur et al., 2015), owing to shallow active layers meaning a limited nutrient pool accessible for plant roots and lower mineralization rates due to thermal constraints. In accordance to this, nutrients added to the active layer in fertilization experiments have been shown to strongly enhance vegetation growth (Natali et al., 2012; Pedersen et al., 2020; Street et al., 2018). In our simulations, historical increases in permafrost organic matter mineralization led to the release of additional N to the active layer, especially in late summer. This N fertilization effects is, however, only minorly impacted the change in GPP, which our results suggest is a consequence of incomplete plant use of the N released in the deep soil.

The incomplete use of increased N supply firstly owes to the mismatch in the timing of simulated peak vegetation growth and soil thaw. Both our model and collected observations show that peak vegetation growth occurs 4–8 weeks earlier than the timing of maximum permafrost thaw, the time period when new nutrients in the deep active soil are mineralized to biologically available compounds. In addition to this, soil conditions only allow for root growth in the deep soil for several weeks in the late summer before the deep soil re-freezes, greatly limiting the potential for deep-soil build-up of root mass. Due to this temporal and spatial mismatch, plants only use around half of increased N mineralised in the deep soil in our model, leading to accumulation of N in the deep soil. Treat et al. (2016) suggest a similar mismatch due to increased N availability in the fall owing to deep-soil thaw, leading to higher biologically available N in the deep soil in this season.

Few studies have assessed seasonal and long-term dynamics of root growth and plant uptake in relation the dynamics of soil thaw. In our model, the vast majority (>85%) of roots are simulated in the top 20-to-30 cm of the soil, which is in accordance to observed vertical root distribution profiles (Blume-Werry et al., 2019; Iversen et al., 2015; Keuper et al., 2020). Since the vegetation is already in senescence by the time the seasonal thaw maximum is reached, the vegetation's investment into root growth is low in the model. However, it remains unclear if these relatively small root fractions in the deep soil (<5% of total root mass) could lead to disproportionate uptake of nutrients in the deeper soil. In the case of *Eriophorum vaginatum*, adapted uptake in the late summer could give the species a competitive advantage in the case of active layer deepening (Blume-Werry et al., 2019). Uptake of deep-soil N in late autumn has also been demonstrated for *Salix arctica* by Pedersen et al. (2020)

through the use of stable isotopes, but overall, the magnitude that a competitive advantage of individual species exhibits at the larger scale still remains enigmatic, since most plant species found in the Arctic Tundra seldomly root past 40 cm depth (Iversen et al., 2015).

Finger et al. (2016) postulate in their analysis of N availability over permafrost thaw gradients that vegetation uses additional N made available through permafrost thaw over time-scales of years to centuries. Thus longer time periods may be needed for plants to adapt to increasing N availability in the deeper permafrost-affected soil. A key uncertainty in our study is that we cannot resolve with the present observational basis, is the deep-soil uptake rate of N by plants, which could be dictated by adaptation abilities of the vegetation to increase their rooting depth with increasing soil thaw.

4.4 | Implications for N loss pathways and N_2O emissions

Due to the incomplete use of deep active layer nutrients by plants, our model shows accumulation of both biologically available N near the permafrost table. Ultimately, three pathways are plausible following increased N concentrations in the deep soil. Either they are mixed into the active soil layer and thus made available for plant uptake over longer timescales (Finger et al., 2016), exported laterally (Treat et al., 2016), or used microbially for denitrification and outgassed as either N_2O or N_2 (Voigt et al., 2020).

Our model suggests an important increase in N loss pathways through nitrification and denitrification, which results in an enhancement of N_2O emissions over the high Arctic. The magnitude in the N_2O emissions increase is dependent on local total soil N, meaning the accumulation is larger with higher N mobilization from the permafrost. Our model also simulates higher loss of N and higher site-level N_2O emission trends with larger trends with deep thawing on average. The limited accessibility of roots to increasingly deeper soil layers could lead to a less N efficient uptake of the deep-soil N, and thus exposing larger amounts of N to other loss pathways. This is illustrated by Cherskiy having a reduced relative response in GPP but higher relative N_2O increase than at Samoylov, with a higher degree of thaw. In turn, our model even suggests a decrease in emissions only at Kangerlussuaq, Greenland (DK-KAN, Figure S2), where thaw depths do not exceed 50 cm, thus providing poor conditions accumulation of N and for production of N_2O.

Since lateral exports remove biogeochemical compounds from permafrost systems, it could affect the potential use of nutrients originating from permafrost thaw by plants and microbes (Treat et al., 2016). Lateral water and biogeochemical exports from the permafrost are, however, still poorly constrained (Lacroix, Ilyina, Mathis, et al., 2021; Lacroix et al., 2020), and difficult to assess in our model-based study. These lateral exports could however have important implications for high-Arctic freshwater systems (Sanders et al., 2022) and Arctic shelves (Dai et al., 2022; Lacroix, Ilyina, Laruelle, et al., 2021; Terhaar et al., 2021).

4.5 | High Arctic as a weak, but emergent source of N_2O gas

N_2O is a strongly potent greenhouse gas and its global budget could impact the global climate in the future (Tian et al., 2020). The magnitude of N_2O emissions from high latitudes has, however, been largely disregarded due to low active layer nutrient contents in these regions (Marushchak et al., 2021). Recent studies that have measured N_2O fluxes at site-level, have reported weak emissions per area in permafrost-affected ecosystems, that could add up to an important component of the global N_2O budget (Voigt et al., 2020), in addition to hot-spot emmissions that could disproportionally affect the N_2O budget in the high latitudes (Marushchak et al., 2021; Wilkerson et al., 2019). The overall magnitude of our present-day N_2O emission average at the high Arctic scale (4 mg N m^{-2} $year^{-1}$) is still around three-fold lower than the reported estimate of 11 mg N m^{-2} $year^{-1}$ of Voigt et al. (2020). However, our averaged growing season emissions at the Arctic scale are close to the median measured over the Yedoma domain by Marushchak et al. (2021), with estimates of Wilkerson et al. (2019) being larger for August emissions for the Alaskan Tundra. Our model shows that high-Arctic N_2O emissions are threefold higher when considering permafrost nutrients and carbon contents, and thus are already driven by historical thaw of the permafrost. The results also suggest pathways leading to N_2O emissions could increase disproportionally with future deeper soil thawing because Arctic plants could have limited access to the newly released nutrients in the deeper soil.

The simulated seasonally changing soil hydrological conditions, and thus changes in soil aeration that are needed for nitrification and denitrification, impact the magnitude of the fluxes. Short aerobic periods are a requisite for nitrification, whereas longer anaerobic timespans are needed for denitrification (Voigt et al., 2020), both of which are simulated at our case studies. However, there remains strong uncertainty in our model in terms of accurately representing soil moisture (Figure S3), a notable problem for terrestrial biosphere models that remains to be resolved. Our model does, however, reproduce the time of thawing, and ensuing anaerobic conditions in the deep soil. Our results suggest an increase in total nitrification and denitrification following deep-soil thaw in the late summer. The emission peak only takes place later during soil re-freezing, when the soil is aerated again in the model. These simulated temporal dynamics entail substantial uncertainty, and further work is needed to improve observational constraints on magnitudes and seasonality of N fluxes in permafrost-affected soils.

5 | CONCLUSIONS

Our model results show that N release from permafrost thaw since the 1960s leads to a fertilization effect on plant growth and vegetation C uptake. These effects are low in comparison to other

climate-caused perturbations due to two factors backed by both our model simulations and collected observational data:

1. Deep-soil N mineralization and vegetation growth peaks are temporally decoupled, meaning that N released in the deep soil is not available during the time period of the largest plant N demand.
2. Arctic vegetation presently does not invest large resources into deep-soil root growth and uptake, likely owing to the short time window of growth in the deep soil prior to re-freezing. It is, however, debated how well individual species adapt to seasonal and long-term variations in thaw depths and nutrient release in the deep soil.

Both these effects lead to N accumulation near the permafrost table following permafrost thaw, opening N loss pathways in our model, which is of particular importance with respect to N_2O emissions in the high Arctic. Through the mismatch of peak vegetative growth and deep-soil N release, our results offer a mechanistic explanation for a considerable present-day N_2O flux despite generally low biologically-available N concentrations in the active layers of permafrost-affected soils. Our results suggest that N_2O emissions are already driven by the mobilization of permafrost material and could increase disproportionally with the extent of deepening of the active layer, leading to a positive non-carbon climate feedback. Since thawing of permafrost is projected to substantially increase over the next century, our results call for increased efforts to improve the understanding of the fate of N upon permafrost thaw and to improve observational constraints of C-N-P dynamics, and especially of N_2O emissions in the high Arctic.

ACKNOWLEDGMENTS

We acknowledge technical advice and model run scripts provided by Jan Engel. We also acknowledge discussion inputs from Lin Yu. Open Access funding enabled and organized by Projekt DEAL.

FUNDING INFORMATION

FL, MG, PS and JS received funding from Deutsche Forschungsgemeinschaft (DFG), project numbers GO1380/3-1 and SCHA1322/12-1. FL also received funding from European Union's Horizon 2020 project PROVIDE. MG was additionally supported by the European Research Council (ERC) under the European Union's Horizon 2020 research and innovation programme (grant agreement No 951288, Q-Arctic). SZ and SC were supported by the European Research Council (ERC) under the European Union's Horizon 2020 research and innovation programme (grant agreement No 647204; QUINCY) and (Grant Agreement N° 101003536; ESM2025—Earth System Models for the Future). DH and LK received funding from the Deutsche Forschungsgemeinschaft (DFG, German Research Foundation) under Germany's Excellence Strategy—EXC 2037 'CLICCS—Climate, Climatic Change, and Society'—project number: 390683824, contribution to the Center for Earth System Research and Sustainability (CEN) of Universität Hamburg.

CONFLICT OF INTEREST

All authors declare no conflict of interests.

DATA AVAILABILITY STATEMENT

Model results and code, as well as constructed eddy-covariance GPP seasonality, are available under https://doi.org/10.5281/zenodo.6832235.

ORCID

Fabrice Lacroix https://orcid.org/0000-0003-4749-2826
Sönke Zaehle https://orcid.org/0000-0001-5602-7956
Silvia Caldararu https://orcid.org/0000-0001-5839-6480
Jörg Schaller https://orcid.org/0000-0003-1996-0127
Peter Stimmler https://orcid.org/0000-0002-8599-5486
David Holl https://orcid.org/0000-0002-9269-7030
Mathias Göckede https://orcid.org/0000-0003-2833-8401

REFERENCES

Ballinger, T. J., Overland, J. E., Wang, M., Bhatt, U. S., Hanna, E., Hanssen-Bauer, I., Kim, S.-J., Thoman, R. L., & Walsh, J. E. (2020). *Arctic report card 2020: Surface air temperature*. National Oceanic and Atmospheric Administration, Office of Oceanic and Atmospheric Research, Pacific Marine Environmental Laboratory (U.S.); Cooperative Institute for Climate, Ocean, and Ecosystem Studies. https://doi.org/10.25923/gcw8-2z06

Beermann, F., Langer, M., Wetterich, S., Strauss, J., Boike, J., Fiencke, C., Schirrmeister, L., Pfeiffer, E.-M., & Kutzbach, L. (2017). Permafrost thaw and liberation of inorganic nitrogen in eastern Siberia. *Permafrost and Periglacial Processes*, *28*, 605–618. https://doi.org/10.1002/ppp.1958

Biskaborn, B. K., Smith, S. L., Noetzli, J., Matthes, H., Vieira, G., Streletskiy, D. A., Schoeneich, P., Romanovsky, V. E., Lewkowicz, A. G., Abramov, A., Allard, M., Boike, J., Cable, W. L., Christiansen, H. H., Delaloye, R., Diekmann, B., Drozdov, D., Etzelmüller, B., Grosse, G., … Lantuit, H. (2019). Permafrost is warming at a global scale. *Nature Communications*, *10*, 264. https://doi.org/10.1038/s41467-018-08240-4

Blume-Werry, G., Milbau, A., Teuber, L. M., Johansson, M., & Dorrepaal, E. (2019). Dwelling in the deep—Strongly increased root growth and rooting depth enhance plant interactions with thawing permafrost soil. *The New Phytologist*, *223*, 1328–1339. https://doi.org/10.1111/nph.15903

Boike, J., Nitzbon, J., Anders, K., Grigoriev, M., Bolshiyanov, D., Langer, M., Lange, S., Bornemann, N., Morgenstern, A., Schreiber, P., Wille, C., Chadburn, S., Gouttevin, I., Burke, E., & Kutzbach, L. (2019). A 16-year record (2002–2017) of permafrost, active-layer, and meteorological conditions at the Samoylov Island Arctic permafrost research site, Lena River delta, northern Siberia: An opportunity to validate remote-sensing data and land surface, snow, and permafrost models. *Earth System Science Data*, *11*, 261–299. https://doi.org/10.5194/essd-11-261-2019

Boike, J., Nitzbon, J., Anders, K., Grigoriev, M. N., Bolshiyanov, D. Y., Langer, M., Lange, S., Bornemann, N., Morgenstern, A., Schreiber, P., Wille, C., Chadburn, S., Gouttevin, I., & Kutzbach, L. (2018). *Measurements in soil and air at Samoylov Station (2002–2018)*. PANGAEA. https://doi.org/10.1594/PANGAEA.891142

Bruhwiler, L., Parmentier, F. J., Crill, P., Leonard, M., & Palmer, P. I. (2021). The Arctic carbon cycle and its response to changing climate. *Current Climate Change Reports*, *7*, 14–34. https://doi.org/10.1007/s40641-020-00169-5

Burke, E. J., Ekici, A., Huang, Y., Chadburn, S. E., Huntingford, C., Ciais, P., Friedlingstein, P., Peng, S., & Krinner, G. (2017). Quantifying uncertainties of permafrost carbon–climate feedbacks. *Biogeosciences*, *14*, 3051–3066. https://doi.org/10.5194/bg-14-3051-2017

Cai, Q., Wang, J., Beletsky, D., Overland, J., Ikeda, M., & Wan, L. (2021). Accelerated decline of summer Arctic Sea ice during 1850–2017 and the amplified Arctic warming during the recent decades. *Environmental Research Letters*, *16*, 034015.

Caldararu, S., Thum, T., Yu, L., Kern, M., Nair, R., & Zaehle, S. (2022). Long-term ecosystem nitrogen limitation from foliar $\delta^{15}N$ data and a land surface model. *Global Change Biology*, *28*, 493–508. https://doi.org/10.1111/gcb.15933

Caldararu, S., Thum, T., Yu, L., & Zaehle, S. (2020). Whole-plant optimality predicts changes in leaf nitrogen under variable CO_2 and nutrient availability. *The New Phytologist*, *225*, 2331–2346. https://doi.org/10.1111/nph.16327

Canadell, J. G., Monteiro, P. M. S., Costa, M. H., Cotrim da Cunha, L., Cox, P. M., Eliseev, A. V., Henson, S., Ishii, M., Jaccard, S., Koven, C., Lohila, A., Patra, P. K., Piao, S., Rogelj, J., Syampungani, S., Zaehle, S., & Zickfeld, K. (2021). Global carbon and other biogeochemical cycles and feedbacks. In climate change 2021: The physical science basis. In V. Masson-Delmotte, P. Zhai, A. Pirani, S. L. Connors, C. Péan, S. Berger, N. Caud, Y. Chen, L. Goldfarb, M. I. Gomis, M. Huang, K. Leitzell, E. Lonnoy, J. B. R. Matthews, T. K. Maycock, T. Waterfield, O. Yelekçi, R. Yu, & B. Zhou (Eds.), *Contribution of working group I to the sixth assessment report of the intergovernmental panel on climate change* (pp. 673–816). Cambridge University Press. https://doi.org/10.1017/9781009157896.007

Chadburn, S., Burke, E., Essery, R., Boike, J., Langer, M., Heikenfeld, M., Cox, P., & Friedlingstein, P. (2015). An improved representation of physical permafrost dynamics in the JULES land-surface model. *Geoscientific Model Development*, *8*, 1493–1508. https://doi.org/10.5194/gmd-8-1493-2015

Chadburn, S. E., Krinner, G., Porada, P., Bartsch, A., Beer, C., Belelli Marchesini, L., Boike, J., Ekici, A., Elberling, B., Friborg, T., Hugelius, G., Johansson, M., Kuhry, P., Kutzbach, L., Langer, M., Lund, M., Parmentier, F.-J. W., Peng, S., Van Huissteden, K., … Burke, E. J. (2017). Carbon stocks and fluxes in the high latitudes: Using site-level data to evaluate earth system models. *Biogeosciences*, *14*, 5143–5169. https://doi.org/10.5194/bg-14-5143-2017

Dai, M., Su, J., Zhao, Y., Hofmann, E. E., Cao, Z., Cai, W.-J., Gan, J., Lacroix, F., Laruelle, G. G., Meng, F., Müller, J. D., Regnier, P. A. G., Wang, G., & Wang, Z. (2022). Carbon fluxes in the Coastal Ocean: Synthesis, boundary processes, and future trends. *Annual Review of Earth and Planetary Sciences*, *50*(1), 593–626. https://doi.org/10.1146/annurev-earth-032320-090746

de Vrese, P., & Brovkin, V. (2021). Timescales of the permafrost carbon cycle and legacy effects of temperature overshoot scenarios. *Nature Communications*, *12*, 2688. https://doi.org/10.1038/s41467-021-23010-5

de Vrese, P., Stacke, T., Kleinen, T., & Brovkin, V. (2021). Diverging responses of high-latitude CO_2 and CH_4 emissions in idealized climate change scenarios. *The Cryosphere*, *15*, 1097–1130. https://doi.org/10.5194/tc-15-1097-2021

Ekici, A., Beer, C., Hagemann, S., Boike, J., Langer, M., & Hauck, C. (2014). Simulating high-latitude permafrost regions by the JSBACH terrestrial ecosystem model. *Geoscientific Model Development*, *7*, 631–647. https://doi.org/10.5194/gmd-7-631-2014

Elberling, B., Christiansen, H. H., & Hansen, B. U. (2010). High nitrous oxide production from thawing permafrost. *Nature Geoscience*, *3*, 332–335.

Finger, R. A., Turetsky, M. R., Kielland, K., Ruess, R. W., Mack, M. C., & Euskirchen, E. S. (2016). Effects of permafrost thaw on nitrogen availability and plant–soil interactions in a boreal Alaskan lowland. *Journal of Ecology*, *104*, 1542–1554. https://doi.org/10.1111/1365-2745.12639

Fouché, J., Christiansen, C. T., Lafrenière, M. J., Grogan, P., & Lamoureux, S. F. (2020). Canadian permafrost stores large pools of ammonium and optically distinct dissolved organic matter. *Nature Communications*, *11*, 4500. https://doi.org/10.1038/s41467-020-18331-w

Friedlingstein, P., O'Sullivan, M., Jones, M. W., Andrew, R. M., Hauck, J., Olsen, A., Peters, G. P., Peters, W., Pongratz, J., Sitch, S., Le Quéré, C., Canadell, J. G., Ciais, P., Jackson, R. B., Alin, S., Aragão, L. E. O. C., Arneth, A., Arora, V., Bates, N. R., … Zaehle, S. (2020). Global carbon budget 2020. *Earth System Science Data*, *12*, 3269–3340. https://doi.org/10.5194/essd-12-3269-2020

Göckede, M., Kittler, F., Kwon, M. J., Burjack, I., Heimann, M., Kolle, O., Zimov, N., & Zimov, S. (2017). Shifted energy fluxes, increased Bowen ratios, and reduced thaw depths linked with drainage-induced changes in permafrost ecosystem structure. *The Cryosphere*, *11*, 2975–2996. https://doi.org/10.5194/tc-11-2975-2017

Göckede, M., Kwon, M. J., Kittler, F., Heimann, M., Zimov, N., & Zimov, S. (2019). Negative feedback processes following drainage slow down permafrost degradation. *Global Change Biology*, *25*, 3254–3266. https://doi.org/10.1111/gcb.14744

Guimberteau, M., Zhu, D., Maignan, F., Huang, Y., Yue, C., Dantec-Nédélec, S., Ottlé, C., Jornet-Puig, A., Bastos, A., Laurent, P., Goll, D., Bowring, S., Chang, J., Guenet, B., Tifafi, M., Peng, S., Krinner, G., Ducharne, A., Wang, F., … Ciais, P. (2018). ORCHIDEE-MICT (v8.4.1), a land surface model for the high latitudes: Model description and validation. *Geoscientific Model Development*, *11*, 121–163. https://doi.org/10.5194/gmd-11-121-2018

Haag, R. W. (1974). Nutrient limitations to plant production in two tundra communities. *Canadian Journal of Botany*, *52*, 103–116. https://doi.org/10.1139/b74-014

Harris, I. C. (2019). *CRU JRA v1.1: A forcings dataset of gridded land surface blend of climatic research unit (CRU) and Japanese reanalysis (JRA) data; Jan.1901—Dec.2017*. Centre for Environmental Data Analysis. https://doi.org/10.5285/13f3635174794bb98cf8ac4b0ee8f4ed

Holl, D., Wille, C., Sachs, T., Schreiber, P., Runkle, B. R. K., Beckebanze, L., Langer, M., Boike, J., Pfeiffer, E.-M., Fedorova, I., Bolshianov, D. Y., Grigoriev, M. N., & Kutzbach, L. (2019). A long-term (2002 to 2017) record of closed-path and open-path eddy covariance CO_2 net ecosystem exchange fluxes from the Siberian Arctic. *Earth System Science Data*, *11*, 221–240. https://doi.org/10.5194/essd-11-221-2019

Hugelius, G., Bockheim, J. G., Camill, P., Elberling, B., Grosse, G., Harden, J. W., Johnson, K., Jorgenson, T., Koven, C. D., Kuhry, P., Michaelson, G., Mishra, U., Palmtag, J., Ping, C.-L., O'Donnell, J., Schirrmeister, L., Schuur, E. A. G., Sheng, Y., Smith, L. C., … Yu, Z. (2013). A new data set for estimating organic carbon storage to 3 m depth in soils of the northern circumpolar permafrost region. *Earth System Science Data*, *5*, 393–402. https://doi.org/10.5194/essd-5-393-2013

Hugelius, G., Loisel, J., Chadburn, S., & Yu, Z. (2020). Large stocks of peatland carbon and nitrogen are vulnerable to permafrost thaw. *Proceedings of the National Academy of Sciences of the United States of America*, *117*(34), 20438–20446. https://doi.org/10.1073/pnas.1916387117

Iversen, C. M., Sloan, V. L., Sullivan, P. F., Euskirchen, E. S., McGuire, A. D., Norby, R. J., Walker, A. P., Warren, J. M., & Wullschleger, S. D. (2015). The unseen iceberg: Plant roots in arctic tundra. *The New Phytologist*, *205*, 34–58. https://doi.org/10.1111/nph.13003

Jackson, R. B., Canadell, J., Ehleringer, J. R., Mooney, H. A., Sala, O. E., & Schulze, E. D. (1996). A global analysis of root distributions for terrestrial biomes. *Oecologia*, *108*, 389–411. https://doi.org/10.1007/BF00333714

Keuper, F., Dorrepaal, E., van Bodegom, P. M., van Logtestijn, R., Venhuizen, G., van Hal, J., & Aerts, R. (2017). Experimentally increased nutrient availability at the permafrost thaw front selectively enhances biomass production of deep-rooting subarctic peatland species. *Global Change Biology*, *23*, 4257–4266.

Keuper, F., Wild, B., Kummu, M., Beer, C., Blume-Werry, G., Fontaine, S., Gavazov, K., Gentsch, N., Guggenberger, G., Hugelius, G., Jalava, M., Koven, C., Krab, E. J., Kuhry, P., Monteux, S., Richter, A.,

Shahzad, T., Weedon, J. T., & Dorrepaal, E. (2020). Carbon loss from northern circumpolar permafrost soils amplified by rhizosphere priming. *Nature Geoscience*, *13*, 560–565. https://doi.org/10.1038/s41561-020-0607-0

Kittler, F., Burjack, I., Corradi, C. A. R., Heimann, M., Kolle, O., Merbold, L., Zimov, N., Zimov, S., & Göckede, M. (2016). Impacts of a decadal drainage disturbance on surface–atmosphere fluxes of carbon dioxide in a permafrost ecosystem. *Biogeosciences*, *13*, 5315–5332. https://doi.org/10.5194/bg-13-5315-2016

Koven, C. D., Lawrence, D. M., & Riley, W. J. (2015). Permafrost carbon–climate feedback is sensitive to deep soil carbon decomposability but not deep soil nitrogen dynamics. *Proceedings of the National Academy of Sciences of the United States of America*, *112*, 3752–3757.

Kutzbach, L., Wagner, D., & Pfeiffer, E. M. (2004). Effect of microrelief and vegetation on methane emission from wet polygonal tundra, Lena Delta, Northern Siberia. *Biogeochemistry*, *69*(3), 341–362.

Kutzbach, L., Wille, C., & Pfeiffer, E.-M. (2007). The exchange of carbon dioxide between wet arctic tundra and the atmosphere at the Lena River Delta, Northern Siberia. *Biogeosciences*, *4*, 869–890. https://doi.org/10.5194/bg-4-869-2007

Lacroix, F., Ilyina, T., & Hartmann, J. (2020). Oceanic CO_2 outgassing and biological production hotspots induced by pre-industrial river loads of nutrients and carbon in a global modeling approach. *Biogeosciences*, *17*, 55–88. https://doi.org/10.5194/bg-17-55-2020

Lacroix, F., Ilyina, T., Laruelle, G. G., & Regnier, P. (2021). Reconstructing the preindustrial coastal carbon cycle through a global ocean circulation model: Was the global continental shelf already both autotrophic and a CO_2 sink? *Global Biogeochemical Cycles*, *35*, e2020GB006603. https://doi.org/10.1029/2020GB006603

Lacroix, F., Ilyina, T., Mathis, M., Laruelle, G. G., & Regnier, P. (2021). Historical increases in land-derived nutrient inputs may alleviate effects of a changing physical climate on the oceanic carbon cycle. *Global Change Biology*, *27*, 5491–5513. https://doi.org/10.1111/gcb.15822

Martin, A. C., Macias-Fauria, M., Bonsall, M. B., Forbes, B. C., Zetterberg, P., & Jeffers, E. S. (2022). Common mechanisms explain nitrogen-dependent growth of Arctic shrubs over three decades despite heterogeneous trends and declines in soil nitrogen availability. *The New Phytologist*, *233*, 670–686. https://doi.org/10.1111/nph.17529

Marushchak, M. E., Kerttula, J., Diáková, K., Faguet, A., Gil, J., Grosse, G., Knoblauch, C., Lashchinskiy, N., Martikainen, P. J., Morgenstern, A., Nykamb, M., Ronkainen, J. G., Siljanen, H. M. P., van Delden, L., Voigt, C., Zimov, N., Zimov, S., & Biasi, C. (2021). Thawing Yedoma permafrost is a neglected nitrous oxide source. *Nature Communications*, *12*, 7107. https://doi.org/10.1038/s41467-021-27386-2

McGuire, A. D., Lawrence, D. M., Koven, C., Clein, J. S., Burke, E., Chen, G., Jafarov, E., MacDougall, A. H., Marchenko, S., Nicolsky, D., Peng, S., Rinke, A., Ciais, P., Gouttevin, I., Hayes, D. J., Ji, D., Krinner, G., Moore, J. C., Romanovsky, V., … Zhuang, Q. (2018). Dependence of the evolution of carbon dynamics in the northern permafrost region on the trajectory of climate change. *Proceedings of the National Academy of Sciences of the United States of America*, *115*(15), 3882–3887.

Monteux, S., Keuper, F., Fontaine, S., Gavazov, K., Hallin, S., Juhanson, J., Krab, E. J., Revaillot, S., Verbruggen, E., Walz, J., Weedon, J. T., & Dorrepaal, E. (2020). Carbon and nitrogen cycling in Yedoma permafrost controlled by microbial functional limitations. *Nature Geoscience*, *13*, 794–798. https://doi.org/10.1038/s41561-020-00662-4

Natali, S. M., Holdren, J. P., Rogers, B. M., Treharne, R., Duffy, P. B., Pomerance, R., & MacDonald, E. (2021). Permafrost carbon feedbacks threaten global climate goals. *Proceedings of the National Academy of Sciences of the United States of America*, *118*(21), e2100163118. https://doi.org/10.1073/pnas.2100163118

Natali, S. M., Schuur, E. A. G., & Rubin, R. L. (2012). Increased plant productivity in Alaskan tundra as a result of experimental warming of soil and permafrost. *Journal of Ecology*, *100*, 488–498. https://doi.org/10.1111/j.1365-2745.2011.01925.x

Norby, R. J., Sloan, V. L., Iversen, C. M., & Childs, J. (2019). Controls on fine-scale spatial and temporal variability of plant-available inorganic nitrogen in a polygonal tundra landscape. *Ecosystems*, *22*, 528–543. https://doi.org/10.1007/s10021-018-0285-6

Obu, J. (2021). How much of the Earth's surface is underlain by permafrost? *Journal of Geophysical Research: Earth Surface*, *126*, e2021JF006123. https://doi.org/10.1029/2021JF006123

Palmtag, J., Obu, J., Kuhry, P., Richter, A., Siewert, M. B., Weiss, N., Westermann, S., & Hugelius, G. (in review). A high-spatial resolution soil carbon and nitrogen dataset for the northern permafrost region, based on circumpolar land cover upscaling. *Earth System Science Data Discussions*. https://doi.org/10.5194/essd-2022a-8

Palmtag J., Obu, J., Kuhry, P., Siewert, M.M., Weiss, N., & Hugelius, G. (2022). *A high spatial resolution soil carbon and nitrogen dataset for the northern permafrost region. Dataset version 1. Bolin Centre Database*. https://doi.org/10.17043/palmtag-2022-spatial-1

Park, T., Chen, C., Macias-Fauria, M., Tømmervik, H., Choi, S., Winkler, A., Bhatt, U. S., Walker, D. A., Piao, S., Brovkin, V., Nemani, R. R., & Myneni, R. B. (2019). Changes in timing of seasonal peak photosynthetic activity in northern ecosystems. *Global Change Biology*, *25*, 2382–2395. https://doi.org/10.1111/gcb.14638

Pearson, R., Phillips, S., Loranty, M., Beck, P. S., Damoulas, T., Knight, S. J., & Goetz, S. J. (2013). Shifts in Arctic vegetation and associated feedbacks under climate change. *Nature Climate Change*, *3*, 673–677. https://doi.org/10.1038/nclimate1858

Pedersen, E. P., Elberling, B., & Michelsen, A. (2020). Foraging deeply: Depth-specific plant nitrogen uptake in response to climate-induced N-release and permafrost thaw in the high Arctic. *Global Change Biology*, *26*, 6523–6536. https://doi.org/10.1111/gcb.15306

Previdi, M., Smith, K. L., & Polvani, L. M. (2020). Arctic amplification of climate change: a review of underlying mechanisms. *Environmental Research Letters*, *16*, 093003. https://doi.org/10.1088/1748-9326/ac1c29

Rasmussen, L. H., Zhang, W., Ambus, P., Michelsen, A., Jansson, P. E., Kitzler, B., & Elberling, B. (2022). Nitrogen transport in a tundra landscape: The effects of early and late growing season lateral N inputs on arctic soil and plant N pools and N_2O fluxes. *Biogeochemistry*, *157*, 69–84. https://doi.org/10.1007/s10533-021-00855-y

Runkle, B. R. K., Sachs, T., Wille, C., Pfeiffer, E.-M., & Kutzbach, L. (2013). Bulk partitioning the growing season net ecosystem exchange of CO_2 in Siberian tundra reveals the seasonality of its carbon sequestration strength. *Biogeosciences*, *10*, 1337–1349. https://doi.org/10.5194/bg-10-1337-2013

Running, S., Mu, Q., & Zhao, M. (2015). *MOD17A2H MODIS/Terra gross primary productivity 8-day L4 global 500m SIN grid V006* [data set]. NASA EOSDIS Land Processes DAAC. https://doi.org/10.5067/MODIS/MOD17A2H.006

Salmon, V. G., Schädel, C., Bracho, R., Pegoraro, E., Celis, G., Mauritz, M., Mack, M. C., & Schuur, E. A. G. (2018). Adding depth to our understanding of nitrogen dynamics in permafrost soils. *Journal of Geophysical Research: Biogeosciences*, *123*, 2497–2512. https://doi.org/10.1029/2018JG004518

Salmon, V. G., Soucy, P., Mauritz, M., Celis, G., Natali, S. M., Mack, M. C., & Schuur, E. A. G. (2016). Nitrogen availability increases in a tundra ecosystem during five years of experimental permafrost thaw. *Global Change Biology*, *22*, 1927–1941. https://doi.org/10.1111/gcb.13204

Sanders, T., Fiencke, C., Fuchs, M., Haugk, C., Juhls, B., Mollenhauer, G., Ogneva, O., Overduin, P., Palmtag, J., Povazhniy, V., Strauss, J., Tuerena, R., Zell, N., & Dähnke, K. (2022). Seasonal nitrogen fluxes of the Lena River Delta. *Ambio*, *51*, 423–438. https://doi.org/10.1007/s13280-021-01665-0

Schädel, C., Bader, M. K., Schuur, E. A., Biasi, C., Bracho, R., Čapek, P., De Baets, S., Diáková, K., Ernakovich, J., Estop-Aragones, C., &

Graham, D. E. (2016). Potential carbon emissions dominated by carbon dioxide from thawed permafrost soils. *Nature Climate Change*, *6*, 950–953. https://doi.org/10.1038/nclimate3054

Schädel, C., Koven, C. D., Lawrence, D. M., Celis, G., & Garnello, A. J. (2018). Divergent patterns of experimental and model-derived permafrost ecosystem carbon dynamics in response to Arctic warming. *Environmental Research Letters*, *13*, 105002. https://doi.org/10.1088/1748-9326/aae0ff

Schaller, J., Faucherre, S., Joss, H., Obst, M., Goeckede, M., Planer-Friedrich, B., Peiffer, S., Gilfedder, B., & Elberling, B. (2019). Silicon increases the phosphorus availability of Arctic soils. *Scientific Reports*, *9*, 449. https://doi.org/10.1038/s41598-018-37104-6

Schuur, E. A. G., McGuire, A. D., Schädel, C., Grosse, G., Harden, J. W., Hayes, D. J., Hugelius, G., Koven, C. D., Kuhry, P., Lawrence, D. M., Natali, S. M., Olefeldt, D., Romanovsky, V. E., Schaefer, K., Turetsky, M. R., Treat, C. C., & Vonk, J. E. (2015). Climate change and the permafrost carbon feedback. *Nature*, *520*(7546), 171–179. https://doi.org/10.1038/nature14338

Screen, J., & Simmonds, I. (2010). The central role of diminishing sea ice in recent Arctic temperature amplification. *Nature*, *464*, 1334–1337. https://doi.org/10.1038/nature09051

Serreze, M. C., & Barry, R. G. (2011). Processes and impacts of Arctic amplification: A research synthesis. *Global and Planetary Change*, *77*(1–2), 85–96. https://doi.org/10.1016/j.gloplacha.2011.03.004

Street, L. E., & Caldararu, S. (2022). Why are Arctic shrubs becoming more nitrogen limited? *The New Phytologist*, *233*, 585–587. https://doi.org/10.1111/nph.17841

Strauss, J., Schirrmeister, L., Mangelsdorf, K., Eichhorn, L., Wetterich, S., & Herzschuh, U. (2015). Organic-matter quality of deep permafrost carbon—A study from Arctic Siberia. *Biogeosciences*, *12*, 2227–2245. https://doi.org/10.5194/bg-12-2227-2015

Street, L. E., Mielke, N., & Woodin, S. J. (2018). Phosphorus availability determines the response of tundra ecosystem carbon stocks to nitrogen enrichment. *Ecosystems*, *21*, 1155–1167. https://doi.org/10.1007/s10021-017-0209-x

Sulman, B. N., Salmon, V. G., Iversen, C. M., Breen, A. L., Yuan, F., & Thornton, P. E. (2021). Integrating arctic plant functional types in a land surface model using above- and belowground field observations. *Journal of Advances in Modeling Earth Systems*, *13*, e2020MS002396. https://doi.org/10.1029/2020MS002396

Terhaar, J., Lauerwald, R., Regnier, P., Gruber, N., & Bopp, L. (2021). Around one third of current Arctic Ocean primary production sustained by rivers and coastal erosion. *Nature Communications*, *12*, 169. https://doi.org/10.1038/s41467-020-20470-z

Thum, T., Caldararu, S., Engel, J., Kern, M., Pallandt, M., Schnur, R., Yu, L., & Zaehle, S. (2019). A new model of the coupled carbon, nitrogen, and phosphorus cycles in the terrestrial biosphere (QUINCY v1.0; revision 1996). *Geoscientific Model Development*, *12*, 4781–4802. https://doi.org/10.5194/gmd-12-4781-2019

Tian, H., Xu, R., Canadell, J. G., Thompson, R. L., Winiwarter, W., Suntharalingam, P., Davidson, E. A., Ciais, P., Jackson, R. B., Janssens-Maenhout, G., Prather, M. J., Regnier, P., Pan, N., Pan, S., Peters, G. P., Shi, H., Tubiello, F. N., Zaehle, S., Zhou, F., … Yao, Y. (2020). A comprehensive quantification of global nitrous oxide sources and sinks. *Nature*, *586*, 248–256. https://doi.org/10.1038/s41586-020-2780-0

Treat, C. C., Wollheim, W. M., Varner, R. K., & Bowden, W. B. (2016). Longer thaw seasons increase nitrogen availability for leaching during fall in tundra soils. *Environmental Research Letters*, *11*, 064013. https://doi.org/10.1088/1748-9326/11/6/064013

Voigt, C., Marushchak, M. E., Abbott, B. W., Biasi, C., Elberling, B., Siciliano, S. D., Sonnentag, O., Stewart, K. J., Yang, Y., & Martikainen, P. J. (2020). Nitrous oxide emissions from permafrost-affected soils. *Nature Reviews Earth & Environment*, *1*, 420–434. https://doi.org/10.1038/s43017-020-0063-9

Voigt, C., Marushchak, M. E., Lamprecht, R. E., Jackowicz-Korczyński, M., Lindgren, A., Mastepanov, M., Granlund, L., Christensen, T. R., Tahvanainen, T., Martikainen, P. J., & Biasi, C. (2017). Increased nitrous oxide emissions from Arctic peatlands after permafrost thaw. *Proceedings of the National Academy of Sciences of the United States of America*, *114*(24), 6238–6243. https://doi.org/10.1073/pnas.1702902114

Wilkerson, J., Dobosy, R., Sayres, D. S., Healy, C., Dumas, E., Baker, B., & Anderson, J. G. (2019). Permafrost nitrous oxide emissions observed on a landscape scale using the airborne eddy-covariance method. *Atmospheric Chemistry and Physics*, *19*, 4257–4268. https://doi.org/10.5194/acp-19-4257-2019

Winkler, A. J., Myneni, R. B., Alexandrov, G. A., & Brovkin, V. (2019). Earth system models underestimate carbon fixation by plants in the high latitudes. *Nature Communications*, *10*, 885. https://doi.org/10.1038/s41467-019-08633-z

Yang, G., Peng, Y., Abbott, B. W., Biasi, C., Wei, B., Zhang, D., Wang, J., Yu, J., Li, F., Wang, G., Kou, D., Liu, F., & Yang, Y. (2021). Phosphorus rather than nitrogen regulates ecosystem carbon dynamics after permafrost thaw. *Global Change Biology*, *27*, 5818–5830. https://doi.org/10.1111/gcb.15845

Yokohata, T., Saito, K., Takata, K., Nitta, T., Satoh, Y., Hajima, T., Sueyoshi, T., & Iwahana, G. (2020). Model improvement and future projection of permafrost processes in a global land surface model. *Progress in Earth and Planetary Science*, *7*, 69. https://doi.org/10.1186/s40645-020-00380-w

Yu, L., Ahrens, B., Wutzler, T., Schrumpf, M., & Zaehle, S. (2020). Jena Soil Model (JSM v1. 0; revision 1934): A microbial soil organic carbon model integrated with nitrogen and phosphorus processes. *Geoscientific Model Development*, *13*, 783–803. https://doi.org/10.5194/gmd-13-783-2020

Zaehle, S., Ciais, P., Friend, A., & Prieur, V. (2011). Carbon benefits of anthropogenic reactive nitrogen offset by nitrous oxide emissions. *Nature Geoscience*, *4*, 601–605. https://doi.org/10.1038/ngeo1207

Zaehle, S., & Friend, A. D. (2010). Carbon and nitrogen cycle dynamics in the O-CN land surface model: 1. Model description, site-scale evaluation, and sensitivity to parameter estimates. *Global Biogeochemical Cycles*, *24*, GB1005. https://doi.org/10.1029/2009GB003521

Zhang, X., Xu, S., Li, C., Zhao, L., Feng, H., Yue, G., Ren, Z., & Cheng, G. (2014). The soil carbon/nitrogen ratio and moisture affect microbial community structures in alkaline permafrost-affected soils with different vegetation types on the *Tibetan plateau*. *Research in Microbiology*, *165*(2), 128–139. https://doi.org/10.1016/j.resmic.2014.01.002

Zubrzycki, S., Kutzbach, L., Grosse, G., Desyatkin, A., & Pfeiffer, E.-M. (2013). Organic carbon and total nitrogen stocks in soils of the Lena River Delta. *Biogeosciences*, *10*, 3507–3524. https://doi.org/10.5194/bg-10-3507-2013

SUPPORTING INFORMATION

Additional supporting information can be found online in the Supporting Information section at the end of this article.

How to cite this article: Lacroix, F., Zaehle, S., Caldararu, S., Schaller, J., Stimmler, P., Holl, D., Kutzbach, L., & Göckede, M. (2022). Mismatch of N release from the permafrost and vegetative uptake opens pathways of increasing nitrous oxide emissions in the high Arctic. *Global Change Biology*, *28*, 5973–5990. https://doi.org/10.1111/gcb.16345